Journal of Sound and Vibration (1999) **228**(3), 477–509
Article No. jsvi.1999.2428, available online at http://www.idealibrary.com on IDEAL®

ACTIVE CONTROL OF MOVING SOUND SOURCE RADIATION—NUMERICAL MODELLING IN THE SPACE–FREQUENCY AND SPACE–TIME DOMAINS

V. MARTIN†

Laboratoire de Mécanique de Rouen, UPRESA 6104 *du CNRS, INSA de Rouen, Avenue de L'Université BP*08, 76801 *Saint-Etienne du Rouvray Cedex, France*

(*Received* 17 *November* 1998, *and in final form* 23 *April* 1999)

The active noise control of a moving source such as airplanes landing or taking off, trains, cars... cannot be achieved directly by using today's classical control of an immobile source. The method described here consists in installing a secondary source screen in the vicinity of the controlled domain. The screen is made up of source masts (which may each contain only one source) and the control uses a small number of masts chosen according to the primary wave incidence. The control is thus shifted from some masts to others. This study rests on numerical modelling in the frequency and time domains

1. INTRODUCTION

Active noise reduction of a sound field called "primary field", consists of driving secondary acoustic sources, usually loudspeakers, in such a way that they radiate the primary field, always and everywhere in the domain under study with an opposite phase in order for the two fields to cancel each other out. A great number of feasibility studies and applications have arisen from this technique. Closed domains have been largely explored: guided waves in ducts (e.g. references [1, 2]), the passengers' cabin in airplanes (e.g. reference [3–5]), in cars (e.g. reference [6]). A preliminary work currently under study even envisages active control in satellite launchers [7]. Not only in acoustic cavities but also in exterior domains, active noise control is used for immobile sound sources such as electric transformers and, more originally, such as mills. From among the huge amount of work which has been done in this field, it is worth mentioning here electronically controlled acoustic shadow systems [8, 9] and the essential work, as far as this paper is concerned, on the quality of elementary sound field reproduction in part of an unbounded 3-D

† A large part of this work was done at the 'Laboratoire d'Electromagnétisme et d'Acoustique, Ecole Polytechnique Fédérale de Lausanne' in Switzerland where the author spent six months in the team directed by Pr M. Rossi.

0022-460X/99/480477 + 33 $30.00/0

space [10]. It is shown here that the quality of reproduction depends above all on the secondary source locations with regard to the primary source location and the domain to be controlled. In particular, the notion of alignment of these three items is present, if not written. Recently, some papers have been devoted to the case of moving primary source [11] and this article contributes to this issue.

In the neighbourhood of roads, airports or railways the moving sound sources are, of course, cars, planes and trains. While these vehicles follow long trajectories, people in their gardens or homes are only affected by a few cubic meters. Considering the example of a train of very limited length, it is easy to see the difficulty to reduce its external radiation. One sole secondary source could only protect a small volume for a short time because the volume in question does not remain very long in the shadow of the secondary source. At the other extreme a large number of secondary sources installed along the railway could protect all the people who live there but driving them permanently would be complex and probably technologically unfeasible. It is thus, quite natural to envisage the successive control of adjacent sources. From this viewpoint, at each moment in the timescale associated with the vehicle's trajectory, the adjacent sources in question must be always ready to put into effect a high-quality control by anticipation so that the retroactive control, the goal of which is simply to improve the performance, only operates a minor correction when it starts up. The shift from one set of adjacent sources to another is added to the above process of prediction followed by correction. This approach is presented with the help of numerical simulations, limiting ourselves to noises which vary slowly, for example those arising from an airplane landing or taking off. The originality lies in the hybrid prediction–correction strategy which integrates the shift in driving sources and which is modified in its retroactive part by permanently adapting a convergence coefficient to the primary source location.

This paper presents the approach to the problem in two steps. The first, which focuses on the space–frequency aspects, starts with the case where the primary source is located at a variety of positions, yet is immobile at each location. This distant source radiates, locally, a plane wave in a 3-D half-space bounded by a rigid boundary, the simplest model of an exterior domain with the ground. With a view, in the near future, to auto-adapting very few control channels only, numerical experiments provide the theoretical efficiency of a nine-source screen in a particular combination: one source said to be preponderant with its own driving signal, and the set of the eight other sources submitted to the same driving signal. When the preponderant source is aligned with the primary source and the centre of the acoustic domain to be controlled, the combination is really efficient. The notion of secondary source which should follow the primary source arises thereof. The dependence noted has then to be confirmed in a more systematic way by seeking the most efficient source from a 20 source screen. This investigation leads to the idea of secondary sources assembled in masts due to the important influence of the azimuth angle of the primary source. These two previous characteristics, summed up in the notion of "follower masts", make it possible now to insert the shift in the control while the primary source moves along its trajectory and to observe its theoretical efficiency. Given a primary source trajectory and

"measuring" its azimuth, the two or three efficient masts are identified and activated. In a 84 source screen, eight or 12 sources are auto-adapted and provide, in theory, extraordinary attenuations. The frequency-domain numerical experiments described in the first part of the paper open the way for dealing with the problem of the active control of a moving source.

The aim of the second part of the paper is to find the time-domain algorithm likely to control moving source radiation. The geometrical configurations now inserted in numerical simulations will have to be implemented later in laboratory experiments in an anechoic chamber of medium size, before any implementation *in situ*. Therefore, at present, a spherical primary radiation and an unbounded 3-D space are considered. Bearing in mind that the noise taken into consideration here is of broad bandwidth and varies in time, the control should be done by anticipation. With such an approach, the convolution coefficients upstream of each chosen secondary source should change according to the primary source location. When tested, this idea has not yet proved to be good. Moreover, the predetermined convolution coefficients are adapted for particular temperature and humidity conditions which, in fact, always vary. Thus, the coefficient values will probably need correction to a certain extent. These considerations lead to a control by anticipation for each of the secondary sources, knowing the incidence of the primary wave for which they are activated, and one retroactive control for each of the masts. Having defined the hybrid control strategy, the way anticipation control coefficients are calculated is recalled (e.g. reference [12]) as well as the way retroaction is obtained (e.g. references [13, 14]). Some modifications are made for moving sources like an airplane at landing or take-off, numerical information associated with the control strategy given, the shifted window which follows the incident wave, in particular its azimuth, introduced. The results of numerical simulation show the efficiency of the algorithm modified for the present situation and also the efficiency of the control with shifts from one mast to another.

The conclusion summarizes the main ideas described and the performances obtained by simulation, as well as the open questions arising from this new investigation. Thus, the work presented is primarily a set of numerical experiments (Mathematica was the calculation tool used throughout the work) to define a way of dealing with the problem of active control of moving source radiation. It is not time yet to focus on theoretical writing which will later determine the validity domain of the method.

2. MOVING SHADOW IN THE FREQUENCY-DOMAIN

2.1. DESCRIPTION OF THE PROBLEM IN AN ELEMENTARY GEOMETRICAL CONFIGURATION

An acoustic point source radiates a spherical wave (in homogeneous medium). On a small part of the wave front, and sufficiently far from the source, approximation of the plane wave is carried out intuitively. The domain where the wave is considered to be plane increases when the source moves away. Let us consider such a situation, in other words, a small domain and a remote source.

To limit the pressure level in the domain due to this remote primary source, the secondary sources, the radiations of which are also spherical, are required to radiate, in the domain, a plane wave of the same amplitude as the primary wave but in opposite phase. The secondary sources being located only a short distance from it, how can the requirement be met? With one secondary source only and without taking into consideration the natural amplitude decreasing in $1/r$ (r being the distance to the point source), the same considerations as above would have given successful results in a small domain, even tiny if the finite distance is very short. However, the drop in the amplitude is unavoidable. How can this problem, as well as that of a larger domain, be dealt with? In what conditions would the global radiation of a set of secondary sources help? When limiting ourselves to a small number of control channel, how should the sources be grouped?

Thanks to the linearity of the problem, with regards to the acoustic pressure amplitude, the work is carried out with a primary plane wave, the amplitude value of which is given by $|p_0| = 1$.

At the start, the investigation is made with nine sources (Figure 1) and 33 observation points inside the domain, where the pressure level is to be reduced. The primary wave incidence is characterized by azimuth and elevation angles, θ and ψ respectively. For a source located above the ground its elevation is of negative value. The incident wave reflects on the ground (plane $z = 0$). The domain controlled, momentarily at $z = 0$, avoids a stationary system of waves along the z-axis.

2.2. RECALL OF FREQUENCY-DOMAIN OPTIMAL CONTROL AND OPTIMAL ATTENUATION

Consider a circular frequency ω and a harmonic acoustic pressure $p_0(x_\mu, \omega)$ at a microphone located at x_μ. To reduce the primary pressure, a secondary source located at x_s radiates a secondary pressure $p_{sec}(x_\mu, \omega)$ at the microphone, such that the modulus of residual pressure $p_{res}(x_\mu, \omega) = p_0(x_\mu, \omega) + p_{sec}(x_\mu, \omega)$ is less than the primary field modulus. With $\phi(x_S, \omega)$ the frequency-domain driving signal applied to the secondary source and $G(x_S, x_\mu, \omega)$ the frequency response of the same source at microphone x_μ, the secondary pressure is $p_{sec}(x_\mu\, \omega) = G(x_S, x_\mu, \omega)\, \phi(x_S, \omega)$. In

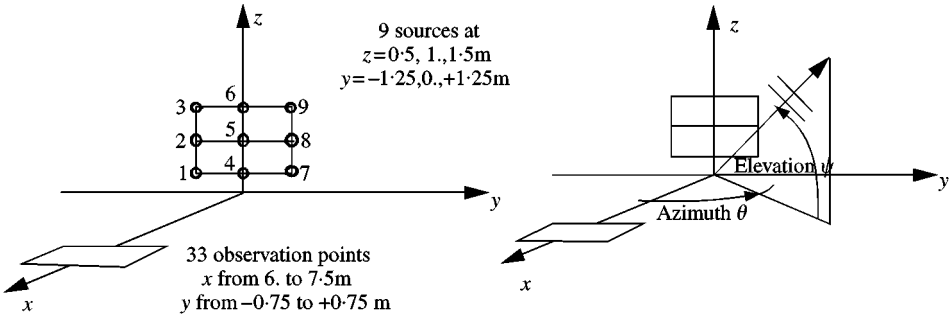

Figure 1. Geometrical configuration of secondary sources and observation points in the controlled domain (on the left) and angles of incidence for the primary wave (on the right).

the presence of more than one secondary source and more than one microphone, the above writings should be understood in the matricial sense.

Optimal frequency-domain control in the sense of the least-mean squares, is the solution of the following programming:

$$\min_{\phi(x_S \cdot \omega)} \| \mathbf{G}(x_S, x_\mu, \omega)\, \phi(x_S, \omega) + \mathbf{p}_0(x_\mu, \omega) \|_{L^2}^2, \tag{1}$$

and its form is

$$\boldsymbol{\phi}^{opt}(x_S, \omega) = -[\mathbf{G}^* \mathbf{G}]^{-1} \cdot \mathbf{G}^* \cdot \mathbf{p}_0(x_\mu, \omega), \tag{2}$$

leading to

$$\mathbf{p}_{sec}(x_\mu, \omega) = -\mathbf{G}[\mathbf{G}^* \mathbf{G}]^{-1} \cdot \mathbf{G}^* \cdot \mathbf{p}_0 = -\mathscr{A} \cdot \mathbf{p}_0, \tag{3}$$

where $\mathscr{A}$ is a projection matrixs (superscript *: conjugate transpose). It results in (for e.g., reference [15])

$$\mathbf{p}_{res}(x_\mu, \omega) = (\mathbf{I} - \mathscr{A}) \cdot \mathbf{p}_0. \tag{4}$$

The frequency-domain optimal attenuation, of positive value, is defined by

$$A_0(\omega) = -10 \log_{10} \frac{\sum_M |p_{res}|^2}{\sum_M |p_0|^2} = -10 \log_{10} \left(1 - \frac{\mathbf{p}_0^* \cdot \mathscr{A} \cdot \mathbf{p}_0}{\mathbf{p}_0^* \cdot \mathbf{p}_0}\right), \tag{5}$$

in the case of M observation points. In the present context, the residual level is $J_{res} = \sum_M |p_{res}|^2 = \mathbf{p}_0^* \cdot (\mathbf{I} - \mathscr{A}) \cdot \mathbf{p}_0$ and the primary level $J_0 = \sum_M |p_0|^2 = \mathbf{p}_0^* \cdot \mathbf{p}_0$. It should be mentioned that frequency-domain optimal control and optimal attenuation are obtained in time-domain through a retroaction which adapts the control (a process also called auto-adaptation of the control) except in very particular cases where the causality is satisfied [12].

2.3. ATTENUATION WITH ONE SOURCE ISOLATED FROM THE OTHERS AND CHOSEN ACCORDING TO THE ANGLES OF THE INCIDENT WAVE

With a view to auto-adapting at a later point to a small number of control channels only, consideration is limited to two different driving signals. How should the sources be assembled so that only two groups are to be dealt with? Two-hundred and fifty-five combinations exist but previous work [10] leads one to consider one isolated source and to drive the other sources with the same signal. Numerical tests run the programming

$$\min_{\phi} J(\phi) = \left\| \left[\left\{ \sum_l G_l \right\} \{G_k\} \right] \boldsymbol{\phi} + \{\mathbf{p}_0\} \right\|_{L^2}^2 \tag{6}$$

to reach the performance. Subscript l refers to the sources with the same driving signal and subscript k is related to the primary wave incidence with the following correspondences:

$$k = 1, \quad \theta = -\arctan(-1{\cdot}25/7), \quad \psi = -\arctan 0{\cdot}5/\sqrt{7^2 + 1{\cdot}25^2},$$

i.e., when the normal to the incident front wave is in the direction of secondary source *no.* 1, seen from centre $\mathbf{x}_c$ of the observation domain;

$$k = 2, \quad \theta = -\arctan(-1{\cdot}25/7), \psi = -\arctan 1{\cdot}0/\sqrt{7^2 + 1{\cdot}25^2},$$

i.e., when the normal to the incident front wave is in the direction of secondary source *no.* 2, seen from centre $\mathbf{x}_c$ of the observation domain;

$$k = 3; \theta = -\arctan(-1{\cdot}25/7), \quad \psi = -\arctan(1{\cdot}5/\sqrt{7^2 + 1{\cdot}25^2}),$$

the normal is in the direction of secondary source no. 3;

$k = 4$, $\theta = 0$, $\psi = -\arctan(0{\cdot}5/7)$, normal in the direction of secondary source no. 4;

$k = 5$, $\theta = 0$, $\psi = -\arctan(1{\cdot}0/7)$, normal in the direction of secondary source no. 5;

$k = 6$, $\theta = 0$, $\psi = -\arctan(1{\cdot}5/7)$, normal in the direction of secondary source no. 6.

Figure 2 shows the optimal attenuation against frequency for various values of k. When $k = 1$–3, the graphs are the same, leading in this case to no influence of the elevation angle. Symmetry considerations make it possible to conclude that the cases $k = 7$–9 would lead to the same graphs (which has been verified). Figure 3 concerns the values of k from 4 to 6 where the attenuations are of high values.

When the isolated sources is on the line going from the primary source to the centre of the controlled domain, the attenuation achieved with two control

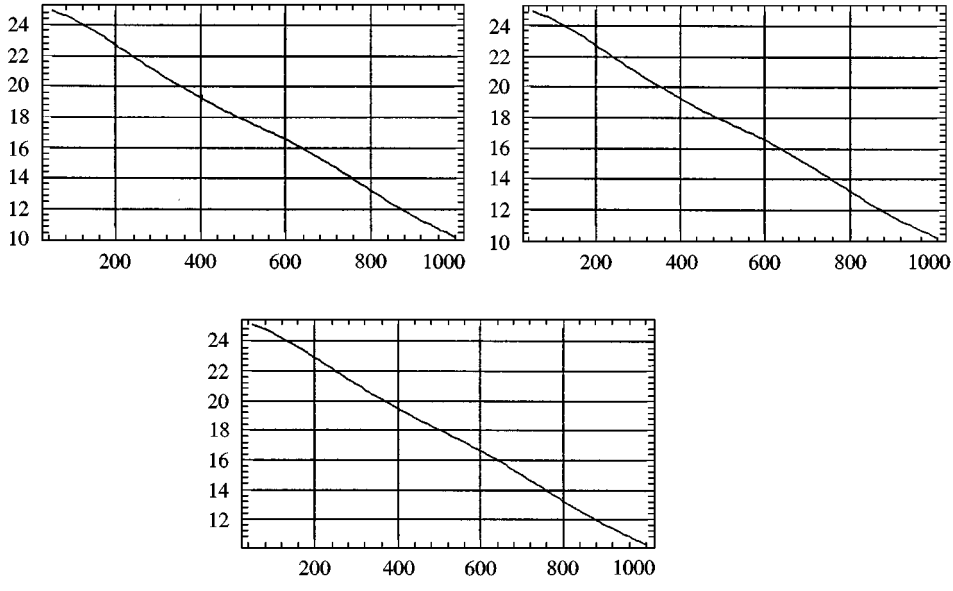

Figure 2. Frequency-domain optimal attenuation obtained when source 1 (top-left), 2 (top-right) or 3 (below) seen from centre x_c of the domain controlled is on the incident wave front normal and when it is isolated from the other sources. Frequency in Hz in abscissa and attenuation in dB in ordinate.

channels only are satisfactory. It already appears here that the results are azimuth dependent rather than elevation dependent. The grounds for these remarks are given more convincingly in the following paragraph.

Just for information, it is worth noting the shadow downstream from the controlled domain at 300 Hz as well as the inception of the stationary system of waves caused by the composition of the primary and secondary waves upstream from the screen for cases $k = 5$ and 7 (respectively, Figures 4 and 5 where the attenuations are of negative value unlike elsewhere in this text).

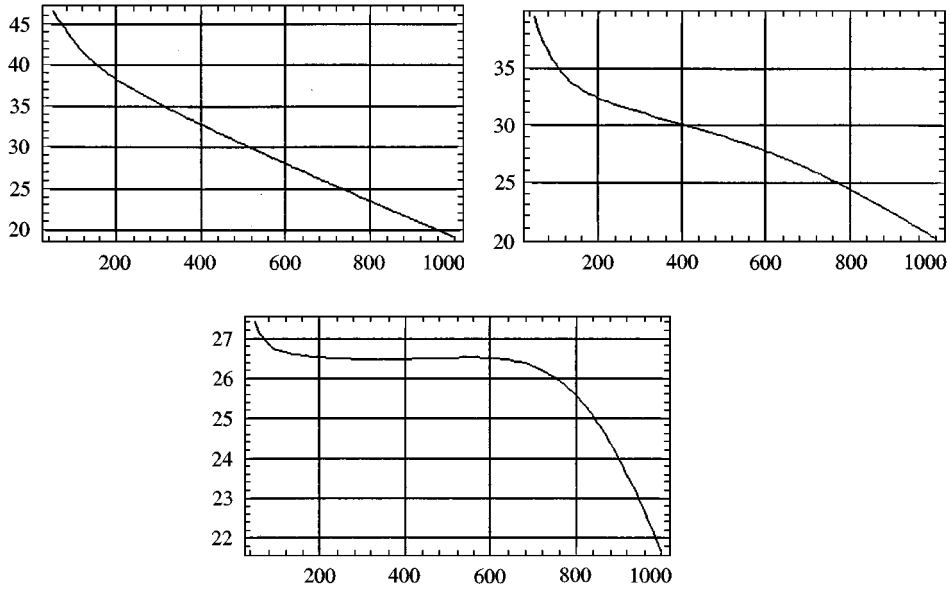

Figure 3. Frequency-domain optimal attenuation obtained when source 4 (top-left), 5 (top-right) or 6 (below) seen from centre x_c of the controlled domain is on the incident wave front normal and when it is isolated from the other sources. Frequency in Hz in abscissa and attenuation in dB in ordinate.

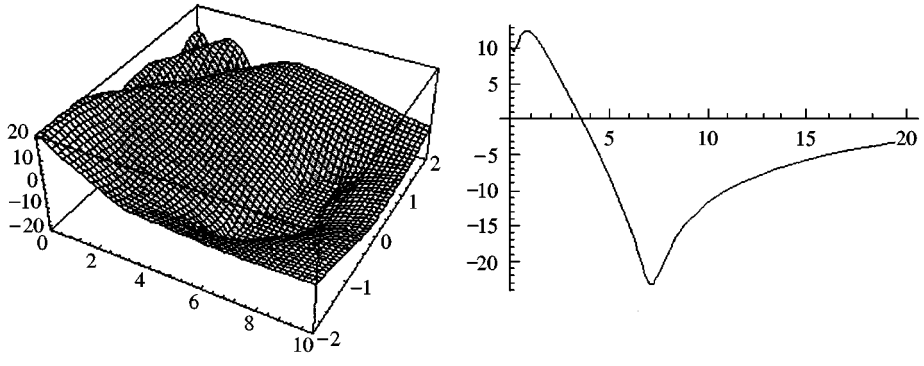

Figure 4. For $k = 5$, shadow downstream from the domain and inception of stationary waves upstream from the screen at 300 Hz. On the left: attenuation in dB against $x \in [0\,\text{m}, 10\,\text{m}]$ and $y \in [-2\,\text{m}, +2\,\text{m}]$. On the right: attenuation in dB against $x \in [0\,\text{m}, 20\,\text{m}]$ at $y = 0$.

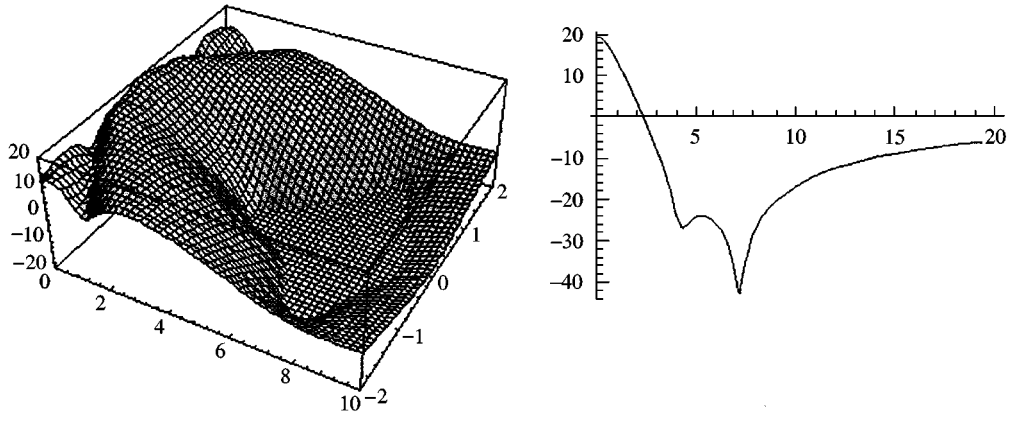

Figure 5. For $k = 7$, shadow downstream from the domain and inception of stationary waves upstream from the screen at 300 Hz. On the left: attenuation in dB against $x \in [0\text{ m}, 10\text{ m}]$ and $y \in [-2\text{ m}, +2\text{ m}]$. On the right: attenuation in dB against $x \in [0\text{ m}, 20\text{ m}]$ at $y = 0$.

2.4. CONSOLIDATION OF THE NOTION OF A SECONDARY SOURCE FOLLOWING THE INCIDENT WAVE

To reinforce the previous notion of "follower" sources, some points must be clarified. First, one should insure that for each incidence, one source (or several sources) appears as being more efficient than the others. Therefore, the information will be of use only if it is possible to predict the said source. It will probably be necessary to add other sources to the most efficient. Here also, is one able to predict the appropriate set of sources? At this level, the numerical experiments indicate the limits of the method. These experiments consist in identifying the most efficient source for various configurations of the domain controlled and for a great deal of primary wave incidences.

The plane screen is now made up of 20 secondary sources, including the nine mentioned previously. The present screen located 50 cm above ground, measuring $5\text{ m} \times 1{\cdot}5\text{ m}$, has five sources along Oy and four along Oz (Figure 6).

For several observation domains (or controlled domains), the sources are classified, by exhaustive means, in the order of decreasing efficiency. To take into account the set of frequencies in the 50–1000 Hz bandwidth, the attenuation indicator is now defined as

$$a'_0 = \sum_{freq} \frac{J_{res}\ (\text{freq})}{J_0\ (\text{freq})}\ . \tag{7}$$

To limit computing costs, the calculation is carried out at 10 frequencies, 100 Hz, apart, ranging from 50 to 950 Hz. In the following tables, the most efficient source can be seen with its resulting attenuation.

Table 1 gives the sources in the order of decreasing efficiency against incidence angles when the controlled domain is the plane domain, given at the beginning of the paper, at $z = 0$ m from 6·5 to 7·5 m along the x-axis, from $-0{\cdot}75$ to $0{\cdot}75$ m along the y-axis, and discretized with 33 points, Here, the most efficient source is

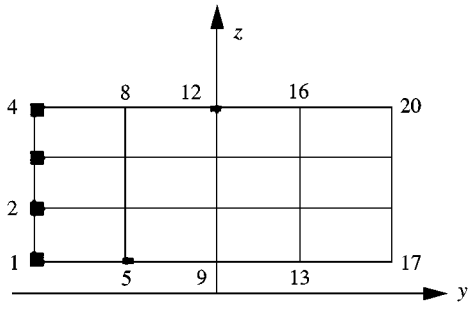

Figure 6. Secondary source numbering for the systematic study of the most efficient source against the primary wave incidence.

TABLE 1

No. of the source acting alone in the order of decreasing efficiency; the observation domain is at $z = 0$

θ azimuth	ψ elevation	Sources
0	$-$ atg (0·5/7)	9 (24–12 dB), 10, 11
	$-$ atg (1·0/7)	10 (24–12 dB), 9, 11
	$-$ atg(1·5/7)	11 (25–12 dB), 10, 12
	$-$ atg(2·0/7)	12 (25–12 dB), 11, 10
atg(1·25/7)	$-$ atg $(0{\cdot}5/(1{\cdot}25^2 + 7^2)^{0{\cdot}5})$	5 (24–12), 6, 7
	$-$ atg $(1{\cdot}0/(1{\cdot}25^2 + 7^2)^{0{\cdot}5})$	6 (25–16), 5, 7
atg (2·5/7)	$-$ atg $(0{\cdot}5/(2{\cdot}5^2 + 7^2)^{0{\cdot}5})$	1 (24–16), 2, 3

undoubtedly located on the radius (defined in the present context, as the line which bears the incident wave front normal) going through the observations domain centre (7, 0, 0). Figure 7 shows the quasi-identical efficiency of sources, the azimuth of which, seen from the centre of the observation domain, is the same as that of the primary wave. As the sources of the identical azimuth are of quasi-identical efficiency, the priority seems to be given to this angle (this remarks was made when it was mentioned that the elevation was of no influence).

Table 2 gives the sources in the order of decreasing efficiency against the incidence angles when the controlled domain is the plane domain, at $z = 1$ m from 6·5 to 7·5 m along the x-axis, from $-0{\cdot}75$ to 0·75 m along the y-axis, and discretized with 33 points. It should be noticed that elevations ψ such that the value of ψ is $-$ atg (1·5/7) (atg means arc tan) or $-$ atg (2·5/7) or $-$ atg $(1{\cdot}5/\sqrt{7^2 + 1{\cdot}25^2})$ or $-$ atg $(2{\cdot}0/\sqrt{7^2 + 1{\cdot}25^2})$ give radii which do not pass through the screen of the secondary sources. Here, the most efficient source is never located on the radius which goes through the centre (7, 0, 1) of the domain. It is to be found at the lowest level of the mast of azimuth θ. In fact, on the mast concerned, the level of most efficient source depends on altitude z (see Table 3). However, in

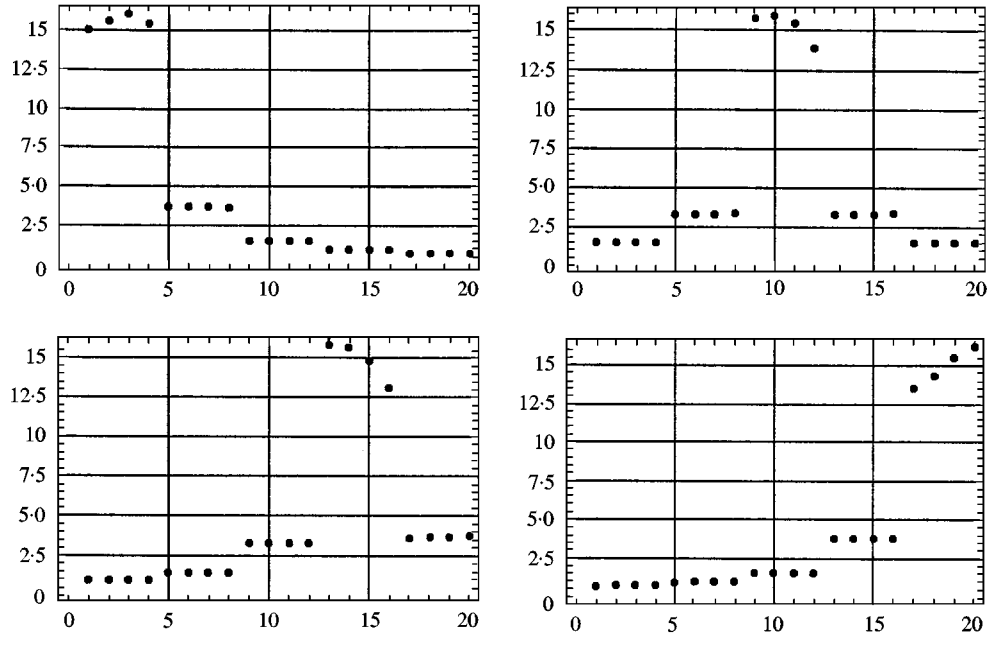

Figure 7. Average optimal attenuation versus the secondary source numbered on the screen in Figure 6, for various incidence of the primary plane wave. The incidences correspond to the angles of a source seen from the centre of the observation domain: top-left: source 3; top-right: source 10; bottom-left: source 13; bottom-right: source 20. In abscissa the source number, in ordinate the average attenuation in dB.

TABLE 2

No. of the source acting alone in the order of decreasing efficiency; the observation domain is at $z = 1$ *m*

θ azimuth	ψ elevation	Sources
0	$-$ atg (0·5/7)	9 (24–16 dB), 11, 10
	$-$ atg (1·0/7)	9 (25–12 dB), 11, 10
	$-$ atg(1·5/7)	9 (25–13 dB), 11, 10
	$-$ atg(2·50/· 7)	9 (254–9 dB), 11, 10
atg(1·25/7)	$-$ atg $(0{\cdot}5/(1{\cdot}25^2 + 7^2)^{0{\cdot}5})$	5 (25–12), 7, 6
	$-$ atg$(1{\cdot}0/(\cdots)^{0{\cdot}5})$	5 (25–11), 7, 6
	$-$ atg $(0{\cdot}5/(\cdots)^{0{\cdot}5})$	5 (24–13), 7, 6
	$-$ atg$(2{\cdot}0)/(\cdots)^{0{\cdot}5})$	5 (25–10), 7, 8
atg(2·5/7)	$-$ atg$(0{\cdot}5/(2{\cdot}5^2 + 7^2)^{0{\cdot}5})$	1 (24–13), 3, 2

these numerical experiments, it has always been observed that the sources located on one mast are of quasi-identical efficiency and to speak of the most efficient does not have a clear significance (Figure 7).

Table 4 gives the sources in the order of decreasing efficiency against incidence angles when the controlled domain is the volume from 6·5 to 7·5 m along the x-axis,

TABLE 3

No. of the source acting alone in the order of decreasing efficiency; the observation domain is at z

θ azimuth	ψ elevation	z	Sources
atg(1·25/7)	$-$ atg(2·0/(1·25^2 + 7^2)$^{0·5}$)	0·25	8, 7, 6, 5
		0·5	6, 5, 8, 7
		1·0	5, 7, 6, 8

TABLE 4

No. of the source acting alone in the order of decreasing efficiency; the observation volume is 0·5 *m above the ground*

θ azimuth	ψ elevation	Sources
0	$-$ atg (0·5/7)	9 (22–3 dB), 10, 13, **12**, 11
	$-$ atg (1·0/7)	10 (22–2 dB), 11, 9, 14
	$-$ atg(1·5/7)	11 (22–2 dB), 12, 10, 15
	$-$ atg(2·50/7)	12 (23–1 dB), 11, 8
atg(1·25/7)	$-$ atg (0·5/(1·25^2 + 7^2)$^{0·5}$)	5 (22–4), 6, 1, 9
	$-$ atg(1·0/(···)$^{0·5}$)	6 (22–2), 7, 5, **8**, 10
atg(2·5/7·)	$-$ atg (0·5/(2·5^2 + 7^2)$^{0·5}$)	1, 2, 5, 3, 4
	$-$ atg(1·0)/(···)$^{0·5}$)	2, 1, 3, 6, 5

from $-$ 0·75 and 0·75 m along the y-axis, from 0·5 to 1·5 m along the z-axis, and discretized with 45 points. Elevations ψ such that the value of ψ is $-$ atg (1·5/7) or $-$ atg (2/7) lead to radii which do not cross the screen. The most efficient source is never on the radius which goes through the volume centre but through the projection of this centre to plane $z = 0$. The other efficient sources are not always in the immediate vicinity of the most efficient one, but are always in the vicinity of the azimuth. The sources numbered in bold type in Table 4 correspond to those farthest from the primary wave incidence.

Table 5 gives the sources in the order of decreasing efficiency against incidence angles when the controlled domain is the off-centre volume from 6·5 to 7·5 m along the x-axis, from $-$ 1·5 to 0 m along the y-axis and from 0·5 to 1·5 m along the z-axis, discretized with 45 points. The most efficient source is always on the radius which goes through the projection of the volume centre on plane $z = 0$. Here also the other efficient sources are not always in the immediate vicinity of the most efficient one—in particular, for extreme elevation—but always on the near azimuth. It is noted that, far away from the incidence azimuth, all the sources are equally inefficient. The sources numbered in bold type in Table 5 correspond to the farthest from the primary wave incidence.

TABLE 5

No. of the source acting alone in the order of decreasing efficiency; the off-centered observation volume is 1 *m above the ground*

θ azimuth	ψ elevation	Sources
atg(− 1·25/7)	− atg(0·5/$\sqrt{\cdots}$)	9 (20–1 dB), 13, **12**, 10, **16**, 14, 11
	− atg(1·0/$\sqrt{\cdots}$)	10 (20–1 dB), 14, 11, 9, 15, 13
	− atg(1·5/$\sqrt{\cdots}$)	11 (21–0 dB), 15, 12, 16, 10, **9**, **13,** 14
	− atg(2·0/$\sqrt{\cdots}$)	12 (22–1 dB), 16, **9**, **13**, 11, 15, 8
atg(1·25/7)	− atg(1·5/$\sqrt{\cdots}$)	1 (20–0 dB), 5, **4**, 2, **8**
	− atg(1·0/$\sqrt{\cdots}$)	2 (20–2 dB), 6, 3, 1, 5
	− atg(1·5/$\sqrt{\cdots}$)	3 (20–2 dB), 7, 4, 2, **1**, 8, 6
	− atg(2·0/$\sqrt{\cdots}$)	4 (22–1 dB), 8, **1**, **5**, 3, 7

2.5. CHOICE IN GROUPING THE SOURCES AND THEORETICAL ATTENUATIONS

From the previous tables, it turns out that the most efficient source always has the same azimuth as the incident wave azimuth, seen from centre $\mathbf{x}_c$ of the observation domain (or from the projection of $\mathbf{x}_c$ on the ground). It is far more difficult to draw conclusions regarding the dependence on the incidence elevation. This is certainly due to the system of stationary waves in the direction of the z-axis brought about by the composition of the incident and reflected waves. It is thus decided to take into account all sources of incidence azimuth and also those the azimuth of which is in their immediate neighbourhood.

The screen is now made up of 84 sources (21 along the y-axis and four along the z-axis) regularly spaced every 0·75 m along Oy and 91·7 m alone Oz. The volume from 6·5 to 7·5 in x, from $-0{\cdot}75$ to $+0{\cdot}75$ m in y, from 0·5 to 1·5 m in z, the discretized with 45 observation points constitutes the controlled domain. The trajectory is defined arbitrarily as a time-function through the dependence of $\psi(t)$ on $\theta(t)$. At each date the incidence, given by $(\theta(t), \psi(t))$, and the observation domain centre define a line crossing the secondary source screen at a point. The set of crossing points forms the projection of the trajectory on the screen. After determining the incidence azimuth, at least two and at most three masts the azimuths of which are nearest to the incidence azimuth are chosen. There are thus at most 12 secondary sources. The graphs in Figure 8 present the optimal attenuations for various frequencies versus the primary source location. The systematic attenuation loss at the centre of the graphs when the azimuth is 0° originates from the space between the masts which is, in appearance, greater here than at the sides of the screen. As the trajectory is not symmetrical with regard to $\theta = 0°$, neither are the attenuations. The high theoretical attenuations obtained with such a system justify the feasibility study which also requires the algorithms to be defined in the time domain in order to cope with the system of sources set-up in masts.

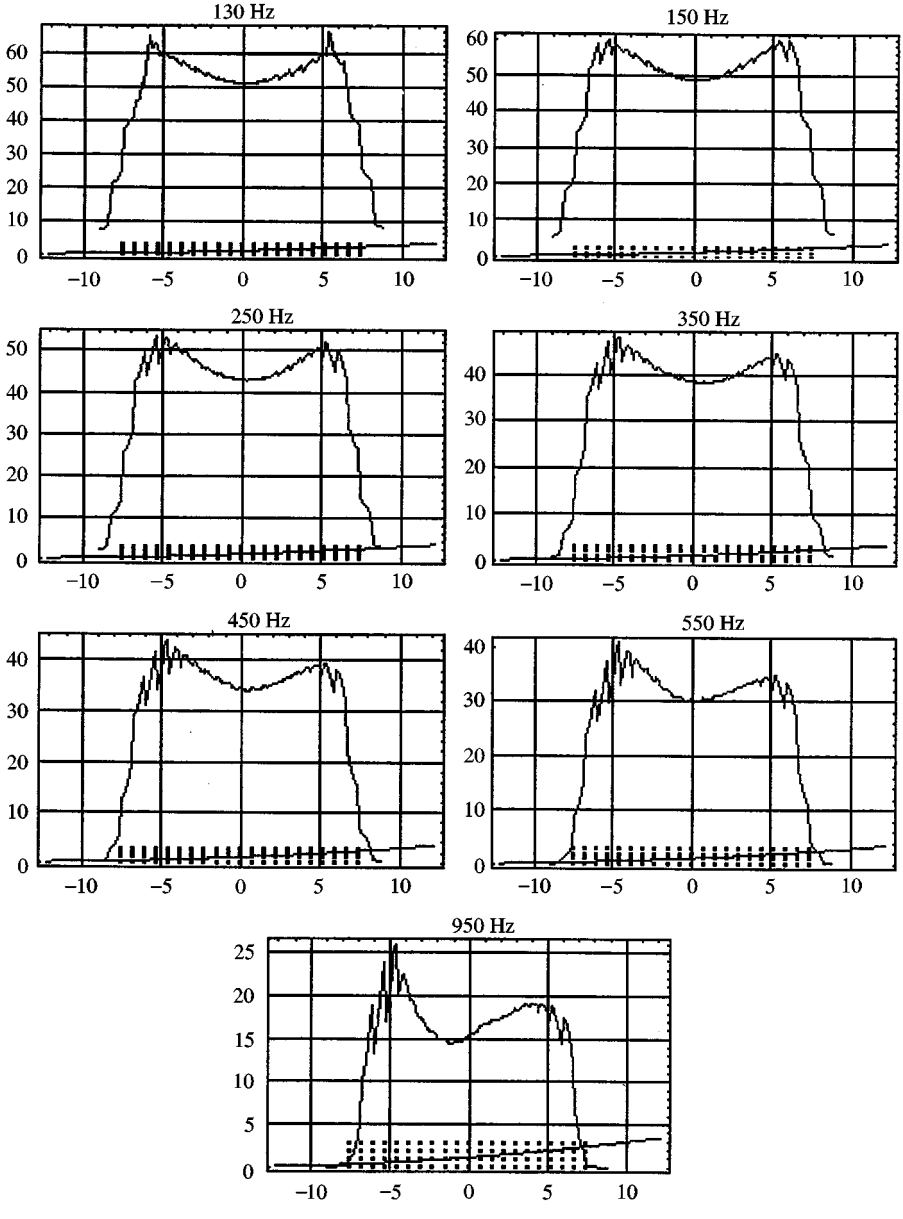

Figure 8. Optimal attenuation in the frequency-domain versus the location of the primary source on its trajectory here projected on the secondary source screen (seen from the controlled domain centre). In abscissa the co-ordinate y in m, in ordinate the attenuation of dB or the height in m; the continuous graphs is the attenuation, the graph superimposed on the sources screen is the trajectory projection; the points represents the sources.

3. TIME-DOMAIN ALGORITHM TO CREATE THE MOVING SHADOW

3.1. GLOBAL STRATEGY

The first part of the paper has shown the importance of all sources the azimuth of which is the incidence azimuth or near it. In other words, in the presence of

a moving primary source, shifts in control from mast to mast will inevitably occur. This point which stems from frequency-domain numerical experiments, has to be clarified in time domain where adequate algorithms are being sought.

Recall that the 12 optimal driving signals in section 2.5 are reachable with 12 auto-adapted channels. To reduce farther the number of such channels, a hybrid control strategy is now envisaged. First, each source of each mast is equipped with a finite impulse response (FIR) filter the predetermined coefficients of which are obtained when the primary source azimuth is that of the mast. Then, the auto-adapted FIR filters concern only the masts activated according to the location of the primary source on its trajectory. Figure 9 illustrates this hybrid strategy in the case of two masts with three secondary sources each. Although the optimal frequency-domain attenuation can probably be calculated for this strategy, we have opted here for the directed study in the time domain.

3.2. RECALLING THE F.I.R. FILTER COEFFICIENT CALCULATIONS FOR CONTROLS BY ANTICIPATION (E.G. REFERENCE [12]

A detection microphone located at x_d indentifies the primary wave. Anticipation consists in predicting the primary field which will arrive at observation microphone x_μ, and in deducing the driving signal which will be applied to the secondary sources to reduce the pressure level at the observation points.

Suppose that, in the time domain, the detector identifies the primary pressure $p_0(x_d, t) = \delta(t - 0)$. Primary pressure $p_0(x_\mu, \omega)$ is predictible if

- there is only one primary source the location x_p of which is known (or its incidence for plane waves radiated);
- it radiation form is known;
- the locations of the observation microphones are known.

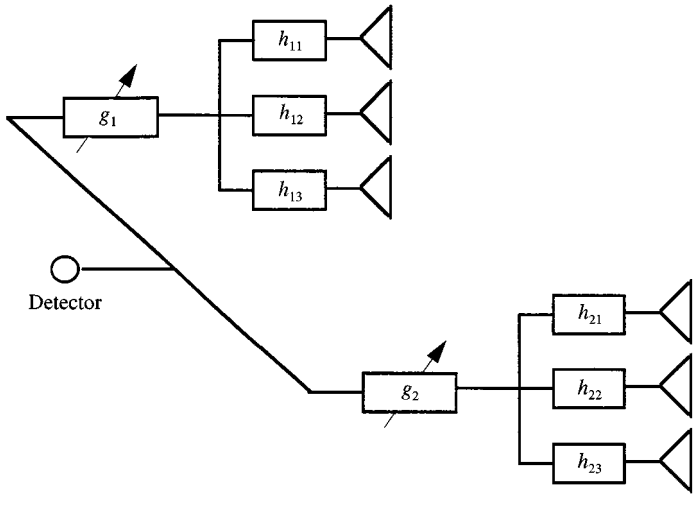

Figure 9. Hybrid active acoustic control strategy with two masts of three sources each; filters h_{ij} are predetermined and filters g_i are adapted.

In the case of a primary source located at x_p and of spherical radiation (Figure 10), one has

$$p_0(x_\mu, t) = \frac{d_1}{d_2(x_\mu)}\,\delta(t - \tau_{d\mu})$$

with

$$\tau_{d\mu} = \frac{d_2(x_\mu) - d_1}{c_0}$$

(c_0 speed of sound in the air) or, in the frequency domain,

$$p_0(x_\mu, \omega) = \frac{d_1}{d_2(x_\mu)}\,\mathrm{e}^{-\mathrm{i}k(d_2(x_\mu) - d_1)}$$

($k = \omega/c_0$ the wavenumber).

The optimal control $\phi_\delta^{opt}(x_s, \omega)$ is reachable (equation (2)) and, via the inverse Fourier transform, $\phi_\delta(x_S, t) = \mathscr{F}^{-1}[\phi_\delta^{opt}(x_S, \omega)]$ (the optimality concept in the frequency domain does not necessarily have the same sense in the time domain and we had rather not mention the optimality in $\phi_\delta(x_s, t)$). It should be noted that inversing the optimal control obtained in the frequency domain may lead to a loss of information as a result of the secondary source response or the responses of elements such as filters presents in the electroacoustic control channel. Underlying this is the causality.

If, now, the detector measures the primary pressure $p_0(x_d, t) = f(t)$, the control to be applied to the secondary source is $\phi(x_s, t) = \phi_\delta(x_s, t)^* f(t)$ (normal writing*: product of convolution) and the resulting secondary pressure is

$$p_{sec}(x_\mu, t) = G(x_s, x_\mu, t) * \phi(x_s, t) \quad \text{with} \quad G(x_s, x_\mu, t) = \mathscr{F}^{-1}[G(x_s, x_\mu, \omega)]. \quad (8)$$

As long as the electroacoustic control channel between the detector and the secondary source (not included) does not have phase-shiftings or amplifications other than those due to the FIR filter, the impulsive response of the latter is

$$h(t) = \phi_\delta(x_S, t). \quad (9)$$

The convolutions leading to $\phi(x_s, t) = \phi_\delta(x_s, t) * (f(t)$ and to $p_{sec}(x_\mu, t) = G(x_S, x_\mu, t) * \phi(x_s, t)$ are discretized with a finite number of points. To this end write

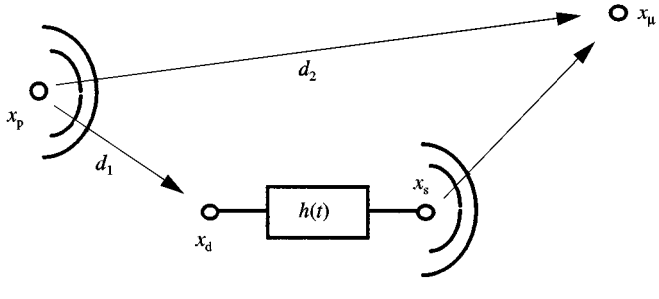

Figure 10. Active acoustic control by anticipation with one secondary source.

$y(t) = h(t) * f(t) = \int_{-\infty}^{+\infty} f(\tau)h(t-\tau)\,\mathrm{d}\tau = \int_{-\infty}^{+\infty} f(t-u)h(u)\,\mathrm{d}u$. When $f(t)$ exists for $t \geqslant t_0$ only, and when $h(t)$ has a finite response for input $\delta(t-0)$, causality imposes that the response cannot exist before the excitation which leads to $h(u) = 0$ for $u < 0$. In these conditions

$$y(t) = \int_{0}^{(t-t_0)>0} f(t-u)\, h(u)\, \mathrm{d}u.$$

Time discretization by steps δt results in the writing of the $(I+1)$ coefficients $h(i)$ in the row vector form $\mathbf{h}^t = \langle h_0, h_1, \ldots, h_I \rangle$ and those of $f(n-\mathrm{i})$ in the column vector form

$$\mathbf{f}_n = \begin{Bmatrix} f_n \\ f_{n-1} \\ \cdots \\ f_{n-I} \end{Bmatrix}.$$

The writing is thus now, $y(n) \approx \sum_{i=0}^{I} f(n-i)\, h(i)$ with $\mathbf{f}_n = 0$ at the start and then filled in FIFO (first in–first out manner). Another writing is

$$y(n) = \mathbf{f}_n^t \cdot \mathbf{h}. \tag{10}$$

Finally, the numerical convolutions computed are, in the case of one secondary source:

$$\phi(x_s, n) = \sum_{i=1}^{n_{11}} h(i)\, f(x_d, n-i) \quad \text{and} \quad p_{sec}(x_\mu, n) = \sum_{i=1}^{n_{12}} G(x_s, x_\mu, i)\phi(x_s, n-i), \tag{11}$$

where the value of n_{11} and n_{12} are determined in such a way that the influences of h and $G_{s\mu}$ can be considered as negligible beyond them.

3.3. RECALL OF RETROACTIVE CONTROL: AUTO-ADAPTATION OF THE MASTS' F.I.R. FILTERS (E.G. REFERENCE [14])

Figure 11 represents one control channel which can be generalized for the present problem. The microphone downstream adds to the perturbation, made up of the primary field $p_0(x_\mu, t)$, the secondary pressure $p_{sec}(x_\mu, t)$ which stems from the electroacoustic channel which comprise one or several secondary sources, followed

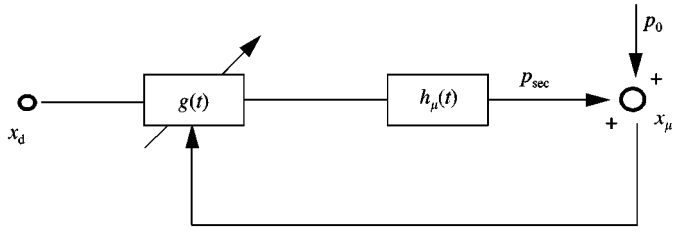

Figure 11. Control channel with retroaction on the coefficients of the FIR filter g.

by the propagation path(s) between the secondary source(s) and the microphone. This microphone, which measures the total or residual pressure is called control microphone. It should be noted that in the controlled domain, observation microphones are not necessarily control microphones. The present goal is to minimize the residual pressure $p_{res}(x_\mu, t)$, and to this end, the coefficients of the FIR filter, called g, will be adapted in order to modify a reference signal, here the pressure $p_0(x_d, t)$ identified at the detector.

So $p_{res}(x_\mu, t) = p_0(x_\mu, t) + h_\mu(t) * g(t) * p_0(x_d, t)$ and, provided a hypothesis is satisfied, $p_{res}(x_\mu, t) = p_0(x_\mu, t) + g(t) * h_\mu(t) * p_0(x_d, t)$. Now, write $rf_\mu(t) = h_\mu(t) * p_0(x_d, t)$, called reference filtered by the secondary path $h_\mu(t)$ made up of the electroacoustic channel followed by the propagation path. After discretization and according to equation (10), the secondary pressure $p_{sec}(x_\mu, t) = g(t) * rf_\mu(t)$ becomes

$$p_{sec}(x_\mu, n) = \langle rf_\mu(n)\ rf_\mu(n-1)\ \cdots\ rf_\mu(n-I)\rangle \begin{Bmatrix} g(0) \\ g(1) \\ \cdots \\ g(I) \end{Bmatrix} = \mathbf{rf}^t_{\mu n} \cdot \mathbf{g}. \tag{12}$$

At each date $n\delta t$, $p^2_{res}(x_\mu, n)$ is a quadratic function of g. Indeed,

$$p^2_{res}(x_\mu, n) = \mathbf{g}^t \cdot \mathbf{rf}_{\mu n} \cdot \mathbf{rf}^t_{\mu n} \cdot \mathbf{g} + 2\ \mathbf{g}^t \cdot \mathbf{rf}_{\mu n} \cdot p_0(x_\mu, n) + p^2_0(x_\mu, n)$$

and there exists an optimal value of $\mathbf{g}$ which minimizes $p^2_0(x_\mu, n)$:

$$\mathbf{g}^{opt} = -(\mathbf{rf}_{\mu n} \cdot \mathbf{rf}^t_{\mu n})^{-1} \cdot \mathbf{rf}_{\mu n} \cdot p_0(x_\mu, n) = -\mathbf{F}^{-1}_{\mu n} \cdot \Phi_{\mu n}$$

or, similarly, $\mathbf{g}^{opt}$ is the vector towards which the following process converges:

$$\mathbf{g}_{new} = \mathbf{g}_{old} - \gamma \nabla_{\mathbf{g}} (p^2_{res}(x_\mu, n)) = \mathbf{g}_{old} - 2\gamma\ \mathbf{rf}_{\mu n} \cdot p_{res}(x_\mu, n).$$

It is decided to work with

$$\mathbf{g}_{n+1} = \mathbf{g}_n - 2\gamma\ \mathbf{rf}_{\mu n} \cdot p_{res}(x_\mu, n), \tag{13}$$

i.e., where the vector at date $(n+1)\,\delta t$ originates from that at date $n\delta t$.

Generalizing the process to M microphones leads to

$$\mathbf{g}_{n+1} = \mathbf{g}_n - \alpha \sum_{\mu=1}^{M} \mathbf{rf}_{\mu n} \cdot p_{res}(x_\mu, n), \tag{14}$$

where α is the (positive) convergence coefficient of the process. This is a cornerstone of the control strategy for a moving source.

3.4. PRELIMINARY TESTS

Result of the simulated retroactive algorithm is verified in the case of the configuration given in Figure 12, analysed in reference [12]. The microphone located at x_d detects the primary signal $f(t)$ brought by the incident primary wave. The coefficients of filter "g" are autoadapted according to equation (14) by using the residual pressure at the control microphones as well as the reference filtered by the secondary paths. n_{xx} associated with a rectangle represents the number of

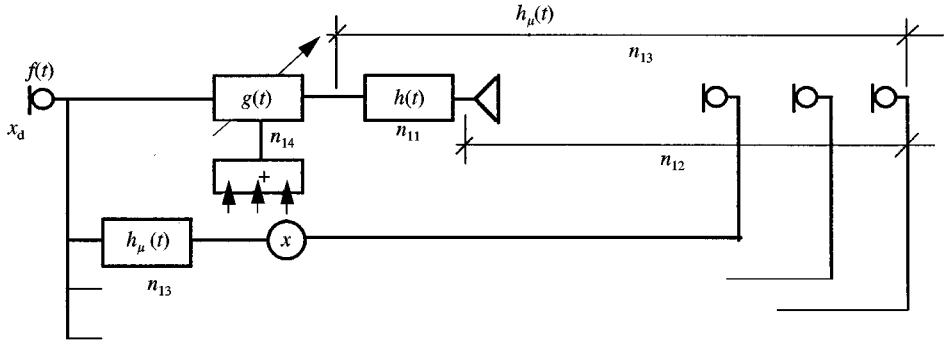

Figure 12. Geometrical configuration of transducers for testing the control by anticipation and retroaction.

coefficients in the FIR filters. n_{xx} alone represents the number of coefficients in the discrete convolution used to simulate the propagations and response in the time-domain.

When the transfer response of the secondary source equals the unity, the anticipatory control gives optimal attenuation. When the secondary source behaviour is correctly modelled, the anticipatory control does not give the optimal attenuation whereas the retroactive control does. This will be verified at 200 Hz. The three observation microphones are also control microphones.

The theoretical optimal attenuation is 11·0 dB (10·9984) whatever the frequency. For the simulation the number of coefficients n_{11} and n_{12} is 409 with a sampling frequency of 8192 Hz. n_{13} is 273 and n_{14} is, almost arbitrarily, 48. It might be surprising that the value of n_{13} is not $n_{11} + n_{12} = 818$, but in this and only this configuration where all transducers are aligned, the filter of impulse response $h(t)$ represents, among others, the opposite of the secondary source response. While the secondary source has a trailing signal after being attacked by an impulse, filter response h followed by the secondary source ideally represents a Dirac signal without any trail. In this configuration, the propagation between secondary source and microphone only adds a pure delay. Thus, n_{11} and n_{12} have to take into account the trailing signal of the secondary source, which is no longer the case for n_{13}.

During the first test, the FIR filter h is neuter that is, $h(t) = \delta(t - 0)$ and paths $\tilde{h}_\mu(t)$, which are estimates of $h_\mu(t)$, only show the transfer between the secondary source and the microphones. The FIR filter $g(t)$, auto-adapted, leads to an optimal attenuation of 11·0 dB (10·9927) for a convergence coefficient at the stability limit, the value of which is $\alpha = 5{\cdot}0/(n_{14} \mid p(x_d, t) \mid^2)$. Figure 13 emphasizes that at each of the three microphones, it takes around 100 ms to reach the minimal residual pressure after the primary field has been established.

During the second test, the impulsive response $h(t)$ of FIR filter h is given in section 3.2. It is known [12] that the global attenuation at 200 Hz obtained by anticipation is 6·3 dB (5·9, 7·4 and 5·9 dB at microphone 1, 2 and 3 respectively). The auto-adapted FIR filter $g(t)$ gives an optimal attenuation of 11·0 dB (10·9925) when the convergence coefficient is $\alpha = 0{\cdot}08/(n_{14} \mid p(x_d, t) \mid^2)$ (at the stability limit;

could this value of α correspond to $0{\cdot}8/((n_{14} + n_{11})\,|\,p(x_d, t)|^2)$. Figure 13 shows at each microphone that, here also, it takes around 100 ms to obtain the minimal residual pressure after the primary field has been established. For each microphone the residual pressure is the same as the first test.

Recall that the filters g and h is series, described for one channel, have a meaning only when generalized to a filter g for each mast and a filter h for each source of each mast, according to the decision made in section 3.1. (and represented in Figure 9) which stems from the results given in the first part of this paper.

3.5. MODIFICATIONS FOR THE ACTIVE CONTROL OF MOVING SOURCE RADIATION

In the presence of both a strategy, justified in the first part of the paper, and an algorithm, which has been verified, the analysis of the moving source in time domain and the notion of a moving weighted window are now introduced. The reasoning used could be qualified of quasi-static as the source moves really slowly, compared to the speed of sound, thus minimizing the Doppler effect.

Figure 14 describes the configuration under study, with the sizing expected to work later with experiments in medium-sized anechoic chamber. The primary

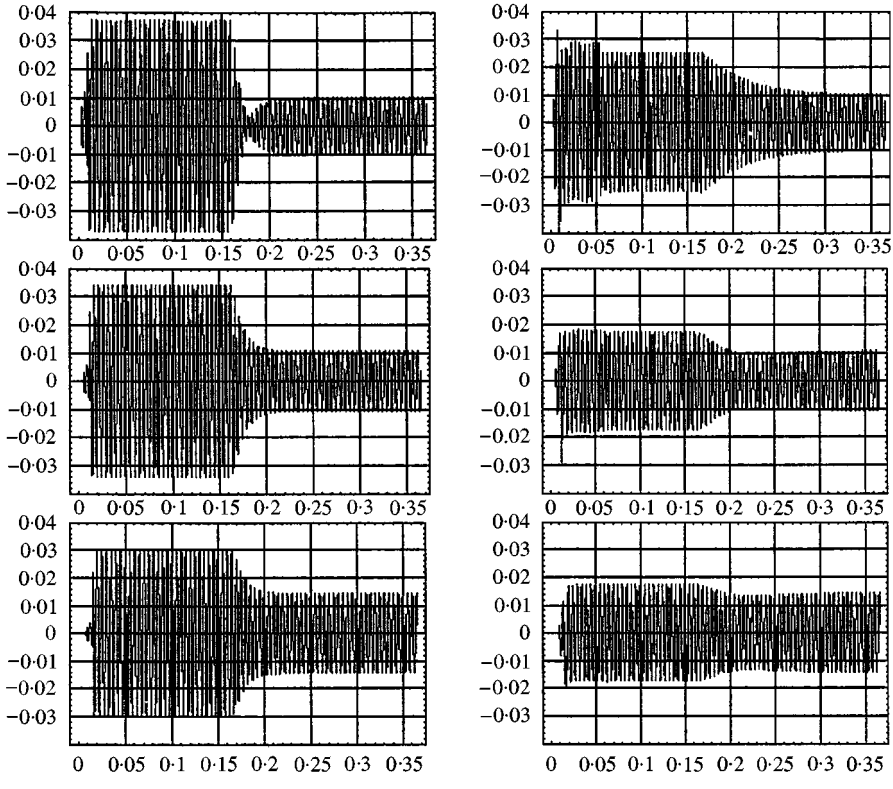

Figure 13. Residual pressure in Pa against time in s at microphones 1–3, from top to bottom. On the left: autoadaptation of filter g with neuter filter h; on the right: autoadaptation of filter g with predetermined filter h.

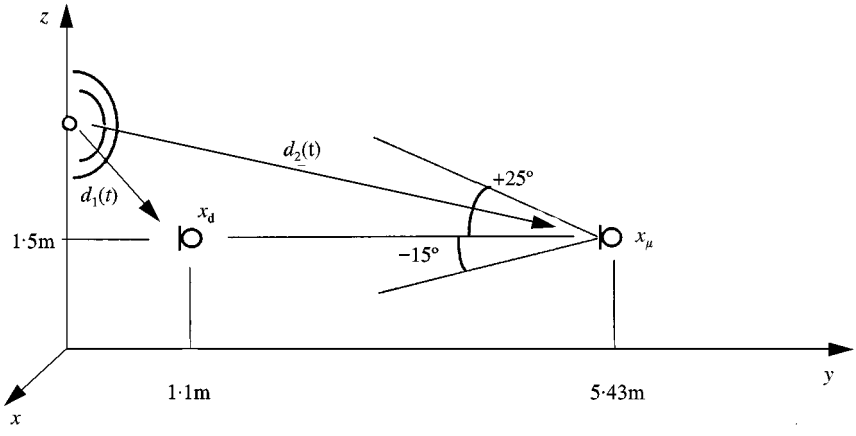

Figure 14. Geometrical configuration for the study of moving source radiation control.

source of spherical radiation follows the trajectory (0, 0, vt) where the source speed is $v = 0{\cdot}65$ m/s. The distance covered when z_s goes from 0 to 4 m lasts 6·15 s. An observer at (0, 5·43, 1·5 m) sees the source moving from angle $-15{\cdot}4$ to $+24{\cdot}7°$, i.e., around 40°. The magnitude orders of the duration and hearing angle of the run are those of a noise radiated by an airplane at take off or landing.

From the starting point at $z_s = 0$ at date $t = 0$, the primary source emits a pressure $q(t)$. After covering the distance $d_1(t)$, distance at date t between source and detector, the pressure arrives at the detector as a signal $f(t) = [1/4\pi\ d_1(t)]$ $q(t - d_1(t)/c)$. In the same manner, with $d_2(x_\mu, t)$ the length at date t from primary source to microphone at x_μ, the primary pressure reaches each microphones with the form

$$p_0(x_\mu, t) = \frac{1}{4\pi\, d_2(x_\mu, t)}\, q\left(t - \frac{d_2(x_\mu, t)}{c}\right) \quad \text{when } t \geqslant \frac{d_2(x_\mu, t)}{c}.$$

In the type of experiments envisaged in the future, the noise amplitude variation due to the distance from primary source to detector will remain weak. Therefore, to approximate variation expected at take off or landing of planes, the source itself is given an emitted signal, the form of which is

$$q(t) = 0{\cdot}2\ \mathrm{e}^{-1/3[z_s(t)-1{\cdot}5]^2} \cos(\omega t).$$

To determine the mast on the radius originating from the primary source and directed towards one point in the controlled domain, the direction of the primary wave is needed. It should be identified simultaneously with the primary signal brought by this wave to the considered point in the domain. However, for causality and technological reasons, the incidence will be identified at the detector at the same date. As, in general, the source trajectory is unknown, one has to accept as a systematic error, the fact of taking for the incidence at the microphone, the incidence at the same date at the detector. This error affects the spatial distribution on the primary field and it will be nevertheless possible, if needed, to obtain the attenuation guaranteed despite its presence [16].

Figure 15 gives the electroacoustic channel suitable for moving source radiation control using the strategy of section 3.1. It is the final form arising from Figures 9–12.

The correction FIR filter $g(t)$ has n_{14} points and the input signal $f(t)$ will thus be ordered in a FIFO of n_{14} points.

Secondary path $\tilde{h}_\mu(t)$, related to each microphone arises from $\tilde{h}_\mu(t) = \mathscr{F}^{-1}\,[\sum_S G_{ms}(x_\mu, \omega)\, h_{ms}(\omega)]$ where the sum on s represents the addition of the sources of the mast, being understood that each transfer $G_{ms}(x_\mu, \omega)$ comprises the frequency response of each source concerned. The simulations presented in this paper will consider sources whose behaviour is described by a localized constants model [17]. If the convolution filters h_{ms} really inverse the source responses, which is the case for ideal sources but not for real sources [12], $\tilde{h}_\mu(t)$ is in fact, the sum of propagation paths in the air. $\tilde{h}_\mu(t)$ is established on n_{13} points.

The voltage applied to the set of sources, noted $v_m(t)$, being convoluted by $h_{ms}(t)$, is stored in a FIFO of n_{11} points. It results in $v_{ms}(t)$, voltage applied to the sources themselves. The latter, being convoluted by $G_{ms}(x_\mu, t) = \mathscr{F}^{-1}\,[G_{ms}(x_\mu, \omega)]$ to simulate through a discrete convolution the secondary pressure emitted by source ms, is thus stored in an n_{12} point FIFO.

The detected signal $f(t)$ is convoluted by the mast convolution filter $g(t)$ and also by $\tilde{h}_\mu(t)$. It must thus be stored on the one hand, in an n_{14} point FIFO and on the other, with n_{13} point FIFO. The output of $\tilde{h}_\mu(t)$ is the filtered reference $rf_\mu(t) = \tilde{h}_\mu(t) * p_0(x_d, t)$. The latter makes it possible to calculate the n_{14} coefficients of g which will be stored (not in a FIFO here) on n_{14} points.

After the geometrical configuration and the electroacoustic channel flow chart with anticipation for the sources and retroaction for the masts, what is now needed for the implementation is the shifting weighted windows which follow the primary source, more precisely its azimuth. One ought to say that the use of spatial weighted

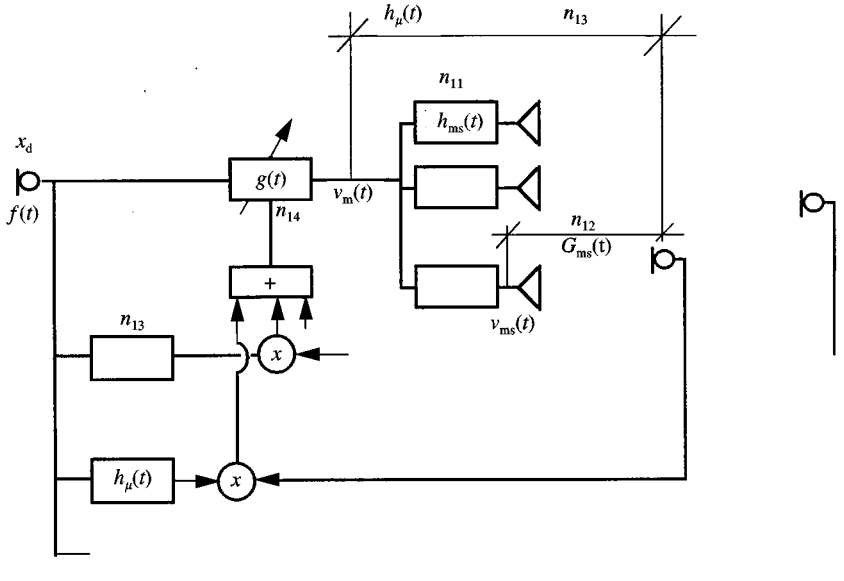

Figure 15. One mast electroacoustic channel of control associated with strategy of Figure 9.

windows is familiar to us in the space and frequency domains for the optimization of secondary source or impedance patch locations [7, 18, 19].

Figure 16 shows the activated masts according to their location within windows F_1, F_2 or F_3 related to the moving source location z_1, z_2 or z_3. In other words, window $F(t)$ shadows primary source location $z(t)$ (or its incidence for which the azimuth plays a vital role).

Once the masts to be activated have been identified by the shifting window, it is not necessary to give then the same importance: according to their locations, near the radius coming from the primary source, or a little farther, it will vary. This consideration leads to a weighted window which acts on the driving signals. At this stage of the feasibility study, the choice is made, *a priori* and without analysis, of a triangular window which provides a gain of one when the mast is on the radius coming from the primary source and which decreases the gain linearly when the mast moves away from this radius. In the presence of two masts only, the gain of the mast are given in Figure 17. At the beginning of the trajectory, the first mast is activated. In the middle, at date t_m, both masts intervene with the same role in the control, and at the end only the second mast is activated. From date t_1 to date t_2, the first mast progressively disappears as it is relayed by the second.

4. TIME-DOMAIN RESULTS

4.1. CASE OF A SOLE MAST WITH TWO SOURCES (I.E., WITHOUT SHIFTING)

4.1.1. *All transducers aligned* (*Figure* 18)

When the primary source is also aligned with the other transducers, this configuration can be solved analytically [12] and the optimal attenuation A_0 reaches 11·00 dB whatever the frequency.

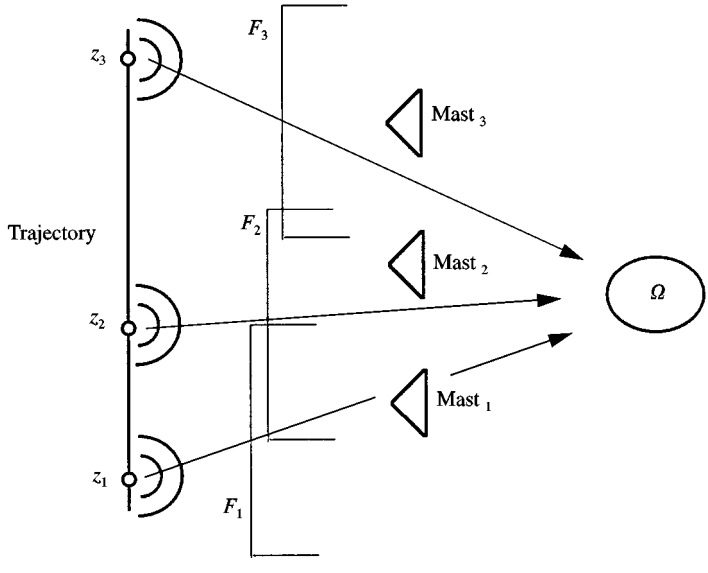

Figure 16. Shifting window F which shadows the primary incidence and activates such or such mast(s).

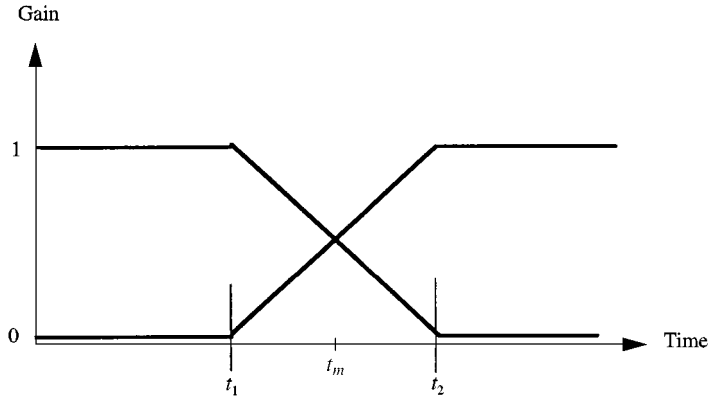

Figure 17. Gain of each mast according to time, i.e., according to the primary source trajectory.

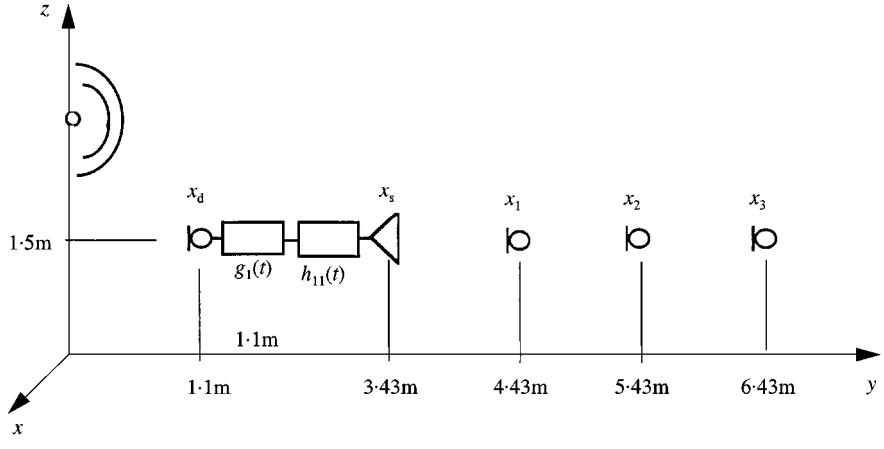

Figure 18. Geometrical configuration where all transducers are aligned and the primary source moving.

Figure 19 shows the evolution in time of the primary pressure and of the residual pressure at microphone $\mathbf{x}_1$ at 200 Hz and 800 Hz. The conditions with which these graphs have been calculated are $n_{11} = 204$, $n_{12} = 81$, $n_{13} = 102$, $n_{14} = 24$, a sampling frequency of 4096 Hz and $\alpha(t) = 0{\cdot}5/(n_{14} | p_0(x_d \cdot t)|^2)$. This latter convergence coefficient which ensures a good compromise between stability and accuracy is always difficult to find. On a PowerBook 3400c the calculation takes around 1 h 20 min. These results and also those, not given here, of the list of attenuations according to azimuth θ, deserves several remarks:

- disregarding the Doppler effect, there exists a symmetry of the attenuations with $\theta = 0°$;
- $h_{11}(t)$ presents an "attack" at 6·84 ms while $6{\cdot}85 \pm 0{\cdot}12$ ms are expected;
- $\tilde{h}(t)$ reveals the good inversion of the secondary source response because its graph is a Dirac (directed towards negative values) at 9·77 ms for microphone

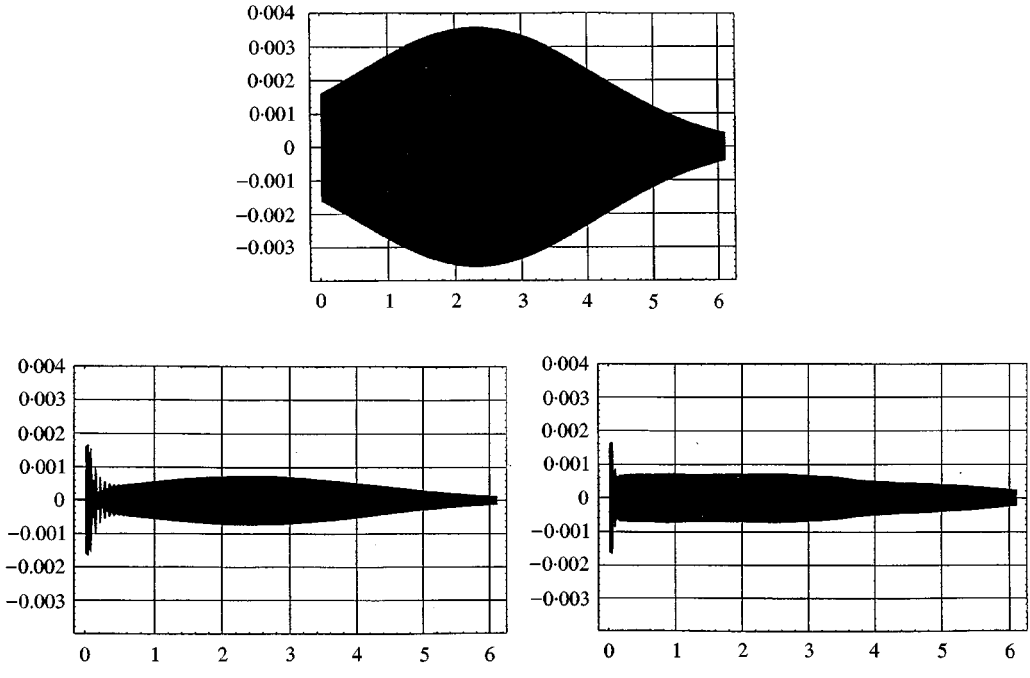

Figure 19. Primary pressure (top) and residual pressure (below) at first microphone versus time, i.e., versus the primary source location on its trajectory; on the left at 200 Hz; on the the right at 800 Hz.

1, 12·71 ms for microphone 2, 15·64 ms for microphone 3, while the expected values are, respectively, 9·79, 12·73 and 15·68 ms, with an error margin or $\pm$ 0.12 ms:

- the expected attenuation of 11 dB for $\theta = 0°$ is well-founded since $A_0(200\text{ Hz}) = 10{\cdot}95$ dB) and $A_0(800\text{ Hz}) = 11{\cdot}02$ dB;
- at 200 Hz, the attenuation is almost the same whatever the primary source location, lying in the interval (8.19, 10·95 dB), the maximal value being at $\theta = 0°$. At 800 Hz, the attenuation variation is far greater, lying in the interval (1·53 and 11·02 dB), the maximum value being at $\theta = 0°$ and the weakest at the end of the trajectory.

4.1.2. *Configuration with four control microphones and one mast of two secondary sources* (*Figure* 20)

Figure 21 shows the evolution in time of the primary pressure and the residual pressure at the third microphone for 200 Hz and at the first microphone for 800 Hz. The graphs were obtained with the following numerical values: $n_{11} = 292$, $n_{12} = 81$, $n_{13} = 136$, $n_{14} = 24$, $F_e = 4096$ Hz. The form of $\alpha(t)$ chosen from among various tests (a time consuming and tedious operation) leads to $\alpha(t) = 0{\cdot}07/(n_{14}\,|\,p_0(x_d,\ t)\,|^2)$ for 800 Hz (we observe that $0{\cdot}07/n_{14} \approx 1/(n_{14} + n_{11})$). At 800 Hz and for $\theta = 0°$, the attenuation obtained is 11·3 dB while the expected value for a fixed source at $z = 1{\cdot}5$ m is 12 dB. At 200 Hz the determination of $\alpha(t)$ turns out to be far more delicate. Indeed, at the beginning of the trajectory, a weak value

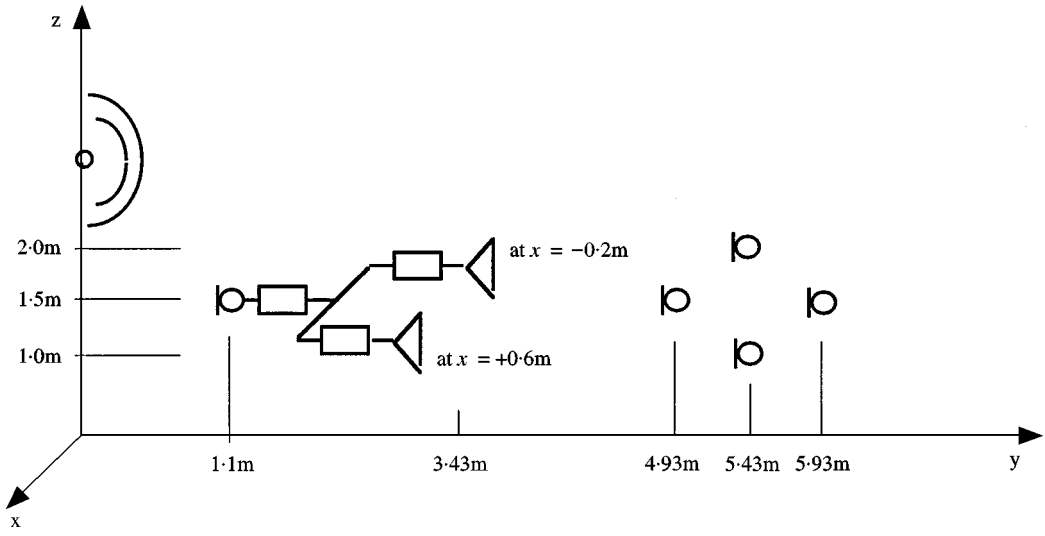

Figure 20. Geometrical configuration with one masts of two sources and four control microphones.

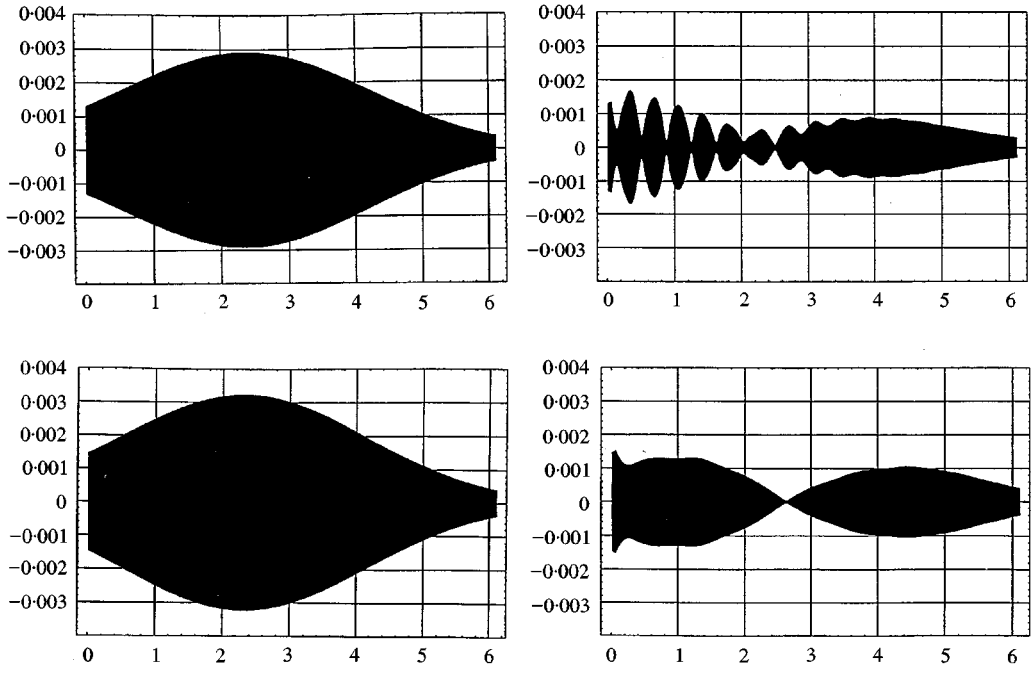

Figure 21. Primary pressure and residual pressure versus time, i.e., versus the primary source location on its trajectory. Top: at microphone 3 at 200 Hz primary pressure (left) and residual pressure (right). Below: at microphone 1 at 800 Hz primary pressure (left) and residual pressure (right).

of α is needed to ensure stability. But this weak value does not enable us to reach the optimal attenuation when $\theta = 0^\circ$. In other words, the optimal attenuation at this azimuth needs a larger value of α, which would destabilize the adaptation loop at the beginning of the trajectory. The compromise is thus, a limit value of α for the

trajectory start and a good performance at azimuth $\theta = 0^\circ$. With these considerations, the form $\alpha(t) = 0{\cdot}03/(n_{14}\,|\,p_0\,(x_d,\ t)|^2)$ results in 14 dB for $\theta = 0$ instead of the optimal value 23 dB. The drawing of residual pressure at microphone 3 for 200 Hz reveals the stability problem at the start of trajectory, the performance at azimuth $\theta = 0^\circ$ and the solidity of the algorithm at the end of the trajectory. Finally, this numerical experiment has shown that the dependence of $\alpha\,(t)$ on time is not the best one and it is an open problems to find a more accurate dependence. On a PowerBook 3400c the calculations last around 3 h.

Had the four microphone been installed at the corners of a square instead of the corners of a diamond, the optimal attenuation $A_0(\omega)$ would have been infinite because, in this configuration, each of the secondary sources would have had the same response at two microphones with the same y-co-ordinate. From the acoustical point of view, the situation would have been that of two secondary sources and two microphones, leading naturally to an infinite attenuation.

For this numerical experiment, several characteristics deserve to be mentioned:

- the driving signals for both sources present the same type of variation according to frequency;
- one of the two FIR filters h has a predominant trail during a long time;
- the FIR filter h associated with the secondary source at $x = -0{\cdot}2$ m provides a delay of 6·84 ms, the one associated with secondary source at $x = +0{\cdot}6$ m, a delay of 6·60 ms. In the present geometrical configuration, the delay derives not only from the distance between detector and secondary source but also from secondary source and controlled domain (Figure 22). Source at $x = +0{\cdot}6$ m has to be driven sooner than source at $x = 0{\cdot}2$ m.
- $\tilde{h}_\mu(t)$ has the form of a Dirac directed towards the negative values superimposed on an oscillation of non-negligible amplitude (Figure 23). The physical interpretation of $\tilde{h}_\mu(t)$ is not obvious as soon as the mast has two or more sources;
- at 800 Hz, the expected symmetry is obtained which is not the case for 200 Hz due the stability limit at the start of the trajectory.

4.2. TWO MASTS OF ONE OR TWO SOURCES EACH (WITH SHIFTING)

4.2.1. *Two masts with one source each*: *control microphones configuration of section* 4.1.1. *with one mast alone at* $z = 1{\cdot}1$ *m, then one at* $z = 2{\cdot}2$ *m, and finally with both masts and with shifting*

The goal of this paragraph consists in verifying that the first mast with its source is efficient at the start of the run, that the second mast is efficient at the end of the run and that both masts combine their effects in the middle of the run.

The type of symmetry expected here is now of a different nature in contrast to the previous symmetry. Except for the Doppler effect, is should be noted that the radiation to the microphones at $z = 1{\cdot}5$ m due to the anti-source (secondary source) at $z = 1{\cdot}1$ m would be exactly the same as that due to the anti-source which would have been located at $z = 1{\cdot}9$ m. In this conditions the optimal attenuation brought by the source at $z = 1{\cdot}1$ m when the primary source follows it trajectory along the

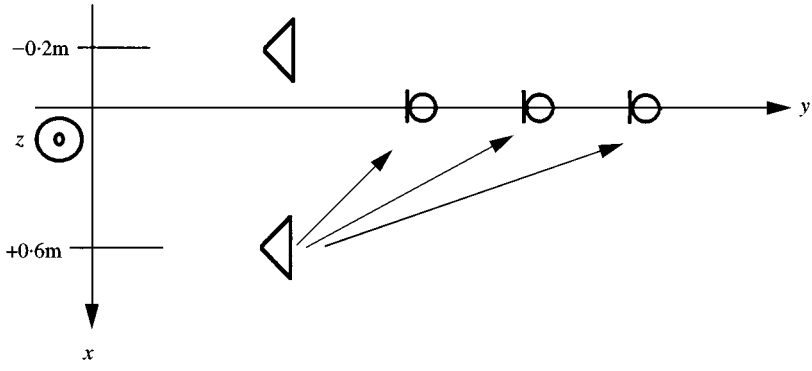

Figure 22. Paths from secondary sources.

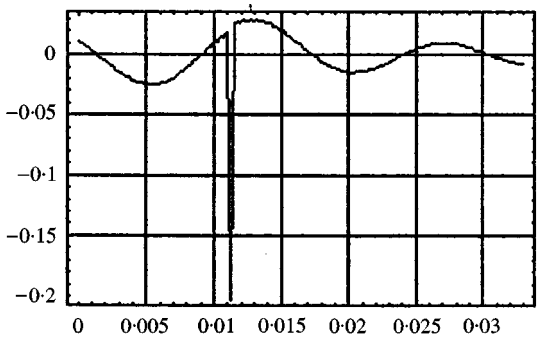

Figure 23. Behaviour of $\tilde{h}_u(t)$ which is not physically self-explanatory is general configurations.

z-axis from 0 to 1·5 m, is the symmetrical relative to $z = 1{\cdot}5$ m of the optimal attenuation when the run is from 1·5 to 3 m. Thus, a symmetry is expected relative to $\theta = 0^\circ$ as long as only one secondary source is activated. With a ground, this symmetry is destroyed.

The number of coefficients n_{11}–n_{14} are, respectively, 204, 81, 102, 24.

At 200 Hz, the secondary source at $z = 1{\cdot}1$ m leads to an expected optimal attenuation of around 11·6 dB when θ is around $-11{\cdot}3^\circ$. With $\alpha(t) = 0{\cdot}5/(n_{14} \mid p_0(x_d \cdot t)\mid^2)$ the attenuation obtained is approximately 11·5 dB at the start of the run. The attenuations contained in the interval (9·6 dB, 11·5 dB) throughout the trajectory, strengthens the fact, seen at section 4.1.1, that at this frequency, good attenuation is obtained whatever the primary source location on its trajectory. Here the shift from one mast to another is hardly justified, if not to verify the behaviour of the shifting algorithm.

On the contrary, at 800 Hz (Figure 24 top-left) the value $\alpha(t) = 0{\cdot}5/(n_{14} \mid p_0(x_d, t)\mid^2)$ taken from section 4.1.1, leads to a divergence for $z = 2{\cdot}2$ m where the value of $\alpha(t)$ had to be decreased to $\alpha(t) = 0{\cdot}3/(n_{14} \mid p_0(x_d, t\mid^2)$. For the sake of coherence, the work was carried out here where $z = 1{\cdot}1$ m, with the latter value of $\alpha(t)$. The secondary source at $z = 1{\cdot}1$ m leads to an expected attenuation of 11·12 dB for

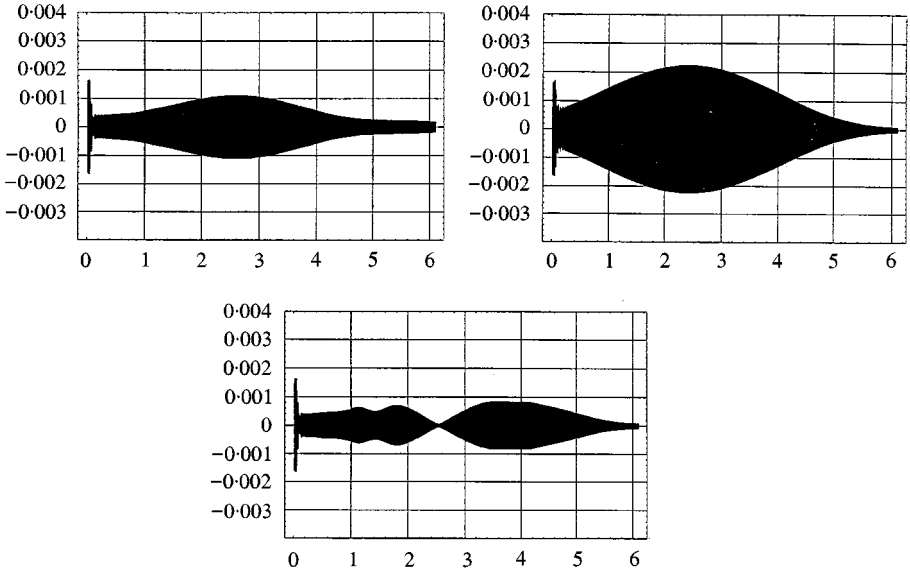

Figure 24. Residual pressure in Pa versus time in s at microphone 1 at 800 Hz (primary pressure given Figure 19). Top-left: the mast at $z = 1{\cdot}1$ m is activated; top-right: the mast at $z = 2{\cdot}2$ m is activated; below: with shift from one mast to the other. From 0 to 1 s and from 5 to 6·3 s one mast activated; from 1 to 5 s both masts radiate and are more efficient from 1 to 4 s than from 4 to 5 s.

$\theta = -11{\cdot}3°$. The expected symmetry is observed and the attenuation obtained at the start is around 11·0 dB. The interval of the attenuations is (3·42 dB, 11·25 dB) throughout the trajectory, the weak attenuations occurring at the end of the run. On a PowerBook 3400c the calculations take around 1 h 20 min.

Still at 800 Hz with the secondary mast (source) now at $z = 2{\cdot}2$ m, the expected optimal attenuation is 9·8 dB when the primary source is such that $\theta = +19{\cdot}3°$. In section 4.1.1, the form $\alpha(t) = 0{\cdot}5/(n_{14} \mid p_0(x_d, t)|^2)$ ensured the stability during the run and the performance for $z_s = 0$. Here, for $z = 2{\cdot}2$ m, this value of $\alpha(t)$ causes the divergence at the start. The form $\alpha(t) = 0{\cdot}4/(n_{14} \mid p_0(x_d, t)|^2)$ results in the stability limit at the beginning of the run and divergence at the end. With $\alpha(t) = 0{\cdot}3/(n_{14} \mid p_0(x_d, t)|^2)$, the system is still stable and the observed attenuation is 9·5 dB whereas its expected value was 9·8 dB. The greatest value is a little farther on in the run and reaches 11·2 dB. During the run the interval of attenuations is (2·23 dB, 11·22 dB), the best ones being at the end (Figure 24 top-right).

It is natural to take advantage of the significant reductions obtained at the start of the run with the mast at $z = 1{\cdot}1$ m and at the end of the run with mast at $z = 2{\cdot}2$ m. With $t_1 = 1{\cdot}0$ s and $t_2 = 5{\cdot}0$ s, and a linear interpolation as described previously, it turns out that the significant attenuations are due to the mast at $z = 1{\cdot}1$ m at the start, to the mast $z = 2{\cdot}2$ m at the end, and that both masts activated are really efficient around $\theta = 0°$. However, the price to be paid is in the small interval located between approximately 4 and 5 s when the source at $z = 2{\cdot}2$ m is preponderant too soon, at a time where the first mast was still efficient (Figure 24 bottom). In fact, the results remain interesting because the loss of efficiency appears here at a moment when the primary field is weak. The modification of the shifting interval from 1 to

5·4 s does give globally less satisfactory results. The duration of the calculation of a PowerBook 3400c is of around 1 h 30 min.

4.2.2. *Two masts with two sources each; control microphones configuration of section* 4.1.2

Here also the goal consists in verifying that the first mast of two sources at $z = 1{\cdot}1$ m is efficient at the beginning of the trajectory, that the second mast of two sources is efficient at the end of the run and that they both combine their efforts in the middle. The number of coefficients n_{11}–n_{14} are, respectively, 292, 81, 102, 24.

At 800 Hz, the mast at $z = 1{\cdot}1$ m leads to an expected optimal attenuation of 12·12 dB for $\theta = -11{\cdot}3°$, azimuth associated with the mast location (for information, at 200 Hz, $A_0 = 23{\cdot}76$ dB). With $\alpha(t) = 0{\cdot}07/(n_{14}\,|\,p_0(x_d,\ t)^2)$, the maximum attenuation reached is of 10·2 dB instead of the 12·12 dB in the vicinity of $\theta = -11{\cdot}3°$. As stability is observed, it is probably possible to increase the convergence coefficient slightly (Figure 25 top-left). The calculation takes around 3 h. Several other remarks are worth making:

- the amplitude of the optimal driving signal when the detected signal is a Dirac, is very high ($\geqslant 80$) till 90 Hz;
- the optimal impulse response related to the source at $x = -0{\cdot}2$ m has a short trail, contrarily to the source at $x = +0{\cdot}6$ m. This observation has not yet received a physical interpretation.
- as in the case of section 4.1.2, $\tilde{h}_\mu(t)$ is made up of a Dirac in the negative direction superimposed on an important oscillation.

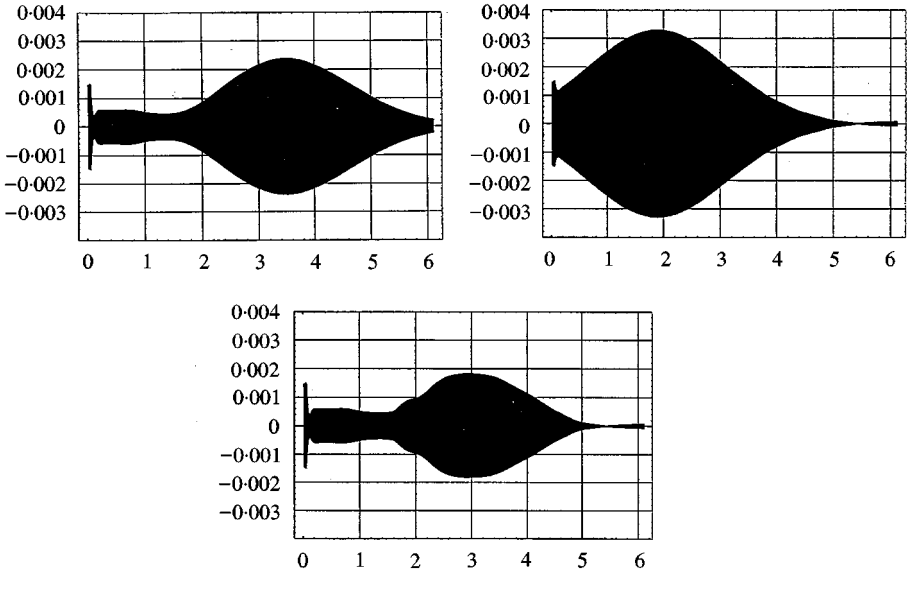

Figure 25. Residual pressure in Pa versus time in s at microphone 1 at 800 Hz (primary pressure given Figure 19). Top-left: the mast at $z = 1{\cdot}1$ m is activated; top-right: the mast at $z = 2{\cdot}2$ m is activated; below: with shift from one mast to the other. From 0 to 1·5 s and from 5 to 6·3 s, one mast activated; from 1·5 to 5 s both masts radiate.

Again at 800 Hz, the mast located at $z = 2{\cdot}2$ m leads to an expected optimal attenuation of 13·38 dB for $\theta = +19{\cdot}3^\circ$, angle associated with the mast location (for information, at 200 Hz, $A_0 = 25{\cdot}07$ dB). With $\alpha(t) = 0{\cdot}07/(n_{14} | p_0(x_d, t)|^2)$, the maximal attenuation reached is 11·5 dB instead of 13·4 dB in the vicinity of $\theta = +19{\cdot}3^\circ$, which suggests here also that the convergence coefficient could be slightly increased as the stability exists (Figure 25 top-right). The other comments are:

- the amplitude of the optimal driving signal when the detected signal is a Dirac, is very high ($\geqslant 80$) till 100 Hz;
- the same characteristics concerning the impulse responses and $\tilde{h}_\mu(t)$ are present.

The shift from the mast at $z = 1{\cdot}1$ m to the mast at $z = 2{\cdot}2$ m with $t_1 = 1{\cdot}5$ s and $t_2 = 5{\cdot}0$ s provides a global attenuation which is always better than the best attenuation obtained with each mast isolated, but without spectacular effects on the attenuation due to the fact that in the latter case each is quite inefficient at that moment (Figure 25 bottom).

5. CONCLUSION

To reduce by active control the deterministic and slowly variable noise radiated by a moving source such as an airplane landing or taking-off, numerical experiments carried out in the frequency domain show that shifting the drive from one secondary source to another or from one mast of sources to another can lead to a good performance, provided that the sources or masts are chosen discerningly according to primary source location. This information which has influenced all the work stems from two numerical experiments. First, being given a nine-source screen and limiting ourselves to two control channels, it appears that one efficient combination consists in isolating the source located on the line which goes in the front primary wave normal direction and goes through one point associated with the acoustic domain to be controlled—for example, the controlled domain centre—, the other sources being submitted to the same driving signal. This observed result, already suggested in 1993 [10] in another context, is here fully exploited. Second, a more systematic work identifies the most important secondary source from among those of a 20 source screen, according to the primary wave incidence. It turns out that the sources located on one mast seen, from the controlled domain, from the same azimuth angle as the primary source, are all quasi-equally efficient and thus, this angle is the main information in the incidence. All this fundamental knowledge leads to a numerical experiment where, according to the primary source azimuth, the two or three masts the azimuth of which are the nearest are activated to show the theoretical attenuations reachable for the configuration: 50, 40, 30, 15 dB at, respectively, 150, 350, 550 and 950 Hz. Such results are motivating and, at this stage, the feasibility study prompts the study of temporal algorithms capable of managing masts and sources.

Another constraint is added to the small number of secondary sources: only a limited number of corrections by retroaction is permitted. This led to a hybrid

strategy of the anticipation–retroaction type, also called prediction–correction. In the first step, the anticipatory control of each source is deduced from information related to the transducers and geometrical configuration which influence the secondary sources radiation. This calculated information has to be replaced, in the real world, by measurements. In the second step, only each set of sources which constitutes a mast is corrected, thanks to a control obtained by retroaction. The strategy and the algorithms being now chosen, some modifications are made to deal with the case of a moving primary source, in particular, the convergence coefficient must be permanently adapted to the primary source location and a weighted window distinguished the active masts on the one hand, and on the other hand modifies the relative importance of the masts taking into account the incident wave azimuth.

Elementary numerical experiments show the efficiency of the hybrid strategy and of the moving shadow in dealing with the problem of a moving source radiation. In particular, the theoretical optimal attenuations resulting from the frequency-domain approach when the azimuth of the activated mast is that of the primary source, are also obtained with the time-domain algorithms when the retroaction loop stability is not a constraint. At 200 and 800 Hz, the attenuations obtained are 10·95 and 11·02 respectively, while the theory announced 11 dB for both frequencies; at 800 Hz, another geometrical configuration leads to 11·3 dB instead of 12 dB, and at 200 Hz, 14 dB instead of 23 dB. Here the convergence coefficient which ensures the stability renders it impossible to reach the theoretical optimal attenuation. On the contrary, the other cases, more favourable, give, at 200 Hz, 11·5 for 11·6 dB expected and at 800 Hz, 11·0 for 11·2 dB, and in other experiments, at 800 Hz, 9·5 for 9·8 dB, 10·2 for 12·12 dB, 11·5 for 13·4 dB.

At the end of this paper, it can be said that the method proposed of feasible. At the objection which might arise from readers who, with legitimate prudence, are on their guard concerning numerical simulation, it is sufficient to mention the results of a previous study [12] on the anticipatory control where experiments conducted at the LEMA-EPFL totally confirmed the expected attenuations, as well as the secondary driving signal.

Beyond the question of feasibility to which a clear answer has ben given, improvements must be brought and open problems investigated further. Among others, the optimization of the driving signal with a constraint on its amplitude calls for a better writing and the insertion of the Doppler effect will make it possible to obtain a better insight for rapid moving sources. From among open problems, primarily depending on optimization theory, what is the law of various of the LMS convergence coefficient according to the primary source location and the detected noise? How can an optimal law of transition be devised to shift from one secondary source mast to another? All these questions will be of even more interest after laboratory experiments have been carried out.

ACKNOWLEDGMENT

The first part of this work was done in the 'Laboratoire CNRS-INSA de Mécanique, Rouen' in France for the EU program "Silence Light" in which

Pr Bernard Nayroles proposed that I participate. The second part, initiated at Rouen, was developed in depth in the acoustic team directed by Pr Mario Rossi at the 'Laboratoire EPFL d'Electromagnétisme et d'Acoustique' in Switzerland during a six month stay. I wish to thank both these close collegues for their enthusiastic encouragement when I told them of my viewpoint on the subject.

REFERENCES

1. A. Roure 1986 *Journal of Sound and Vibration* **101**, 429–441. Self-adaptive broadband active sound control system.
2. P. Sergent and D. Duhamel 1996 *Journal of Sound and Vibration* **207**, 537–566. Optimal placement of sources and sensors with the minimax criterion for active control of a one dimensional sound field.
3. A. J. Bullmore, P. A. Nelson and S. J. Elliott 1990 *Journal of Sound and Vibration* **140**, 191–217. Theoretical studies of the active noise control of propeller-induced cabin noise.
4. S. J. Elliott, P. A. Nelson, I. M. Stothers and C. C. Boucher 1990 *Journal of Sound and Vibration* **140**, 219–238. In-flight experiments on the active control of propeller-induced cabin noise.
5. V. Martin, B. Peseux and Ph. Vignassa 1994 *Journal of Sound and Vibration* **176**, 307–332. Numerical vibroacoustic modelling of aircraft for the acoustic control of interior noise.
6. A. M. McDonald, D. C. Quinn, T. J. Saunders, S. J. Elliott, P. A. Nelson and I. M. Stothers 1998 *The Proceedings of the Institution of Mechanical Engineers Conference on Vehicle Noise*. Adaptive control fo automobile interior noise.
7. V. Martin, A. Bodrero 1997 *Journal of Sound and Vibration* **204**, 331–357. An introduction to the control of sound fields by optimising impedance locations on the wall of an acoustic cavity.
8. S. E. Wright and B. Vuksanovic 1996 *Journal of Sound and Vibration* **190**, 565–585. Active control of environmental noise.
9. S. E. Wright and B. Vuksanovic 1997 *The Proceedings of the* 1997 *Symptosium on the Active Control of Sound and Vibration*, 1135–1148. Publishing Company of Technical University of Budapest. Electronically controlled acoustic shadow systems.
10. O. Kirkeby and P. A. Nelson 1993 *Journal of Acoustical Society of America* **94**, 2992–3000. Reproduction of plane wave sound fields.
11. K. Uesaka, H. Ohnishi, K. Hachimine, M. Nishimura and K. Ohnishi 1997 *The Proceedings of the* 1997 *Symposium on Active Control of Sound and Vibration*, 1125–1134. Publishing Company of Technical University of Budapest. Active control of sound from a moving source.
12. V. Martin, V. Adam and M. Rossi 1998 *Compte-rendu de travaux*, *note interne*, 23 p. Contrôle acoustique actif par anticipation dans un domaine non borné: comparison entre simulations numériques et expériences de laboratoire.
13. C. F. Ross 1982 *Journal of Sound and Vibration* **80**, 381–388. An adaptive digital filter for broadband active sound control.
14. P. A. Nelson and S. J. Elliott 1992 *Active Control of Sound*. New York: Academic Press, (chapter 12.)
15. V. Martin and C. Cariou 1997 *The Proceedings of the* 1997 *Symposium on Active Control of Sound and Vibration*, 673–688. Publishing Company of Technical University of Budapest. Improvement of active attenuation by modifying the primary field.
16. V. Martin and C. Gronier 1998 *Journal of Sound and Vibration* **215**, 827–852. Minimum attenuation guaranteed by an active control system in presence of errors in the spatial distribution of the primary field.

17. M. Rossi 1986 Electroacoustique, Ecole Polytechnique Fédérale de Lausanne. Presses Polytechniques Romandes.
18. B. Nayroles, G. Touzot and P. Villon 1994 *Journal of Sound and Vibration* **171**, 1–21. Using diffuse approximation for optimising the locations of antisound sources.
19. E. Benzaria and V. Martin 1994 *Journal of Sound and Vibration* **173**, 137–144. Secondary source locations in active noise control: selection or optimization?